



Enhanced characterization of oilfield emulsions via NMR diffusion and transverse relaxation experiments

Alejandro A. Peña, George J. Hirasaki*

Department of Chemical Engineering, Rice University, Houston, TX 77005-1892, USA

Abstract

The procedure proposed by Packer and Rees (J. Colloid Interface Sci. 40 (1972) 206) to interpret pulsed field gradient spin-echo (PGSE) experiments on emulsions is commonly used to resolve for the distribution of droplet sizes via nuclear magnetic resonance (NMR). Nevertheless, such procedure is based on several assumptions that may restrict its applicability in many practical cases. Among such constraints, (a) the amplitude of the spin-echo (signal) must be influenced solely by the drop phase, and not by the continuous phase; and (b) the shape of the drop size distribution must be assumed a priori. This article discusses new theory to interpret results from PGSE experiments and a novel procedure that couples diffusion measurements (PGSE) with transverse relaxation rate experiments (the so-called CPMG sequence) to overcome the above limitations. Results from experiments on emulsions of water dispersed in several crude oils are reported to demonstrate that the combined CPMG–PGSE method renders drop size distributions with arbitrary shape, the water/oil ratio of the emulsion and the rate of decay of magnetization at the interfaces, i.e. the surface relaxivity. It is also shown that the procedure allows screening if the dispersion is oil-in-water (*o/w*) or water-in-oil (*w/o*) in a straightforward manner and that it is suitable to evaluate stability of emulsions.

© 2003 Elsevier Science B.V. All rights reserved.

Keywords: Emulsion; Drop size distribution; Nuclear magnetic resonance; CPMG; Pulsed field gradient spin-echo; Surface relaxivity

*Corresponding author. Tel.: +1-713-348-5416; fax: +1-713-348-5478.
E-mail address: gjh@rice.edu (G.J. Hirasaki).

Contents

1. Introduction	104
2. CPMG experiment: basic theory and interpretation	105
2.1. Description of the test	105
2.2. Determination of drop sizes in emulsions via CPMG	106
2.3. Range of drop sizes that can be resolved via CPMG	107
2.4. Determination of the water/oil composition in emulsions	109
3. PGSE experiment: basic theory and interpretation	110
3.1. Description of the test	110
3.2. Determination of drop sizes in emulsions via PGSE	111
3.3. A novel theory to resolve PGSE data in the time domain	115
3.4. Range of drop sizes that can be resolved via PGSE	117
4. Combined CPMG-PGSE method	119
4.1. Advantages and limitations of the CPMG experiment	119
4.2. Advantages and limitations of the PGSE experiment	119
4.3. Combining experimental data from both methods	120
5. Computational procedures	121
6. Experimental	122
7. Results and discussion	124
7.1. Properties of the pure fluids	124
7.2. Validation of Eq. (32)	126
7.3. The combined CPMG–PGSE method in practice	130
7.4. Morphology of the emulsion	139
7.5. Oil/water composition	139
7.6. Surface relaxivities	141
8. Conclusions	142
Acknowledgements	143
Appendices	143
References	146

1. Introduction

An emulsion is a relatively stable dispersion of drops of one liquid (the *drop phase*) into another liquid (the *continuous phase*) with which it is immiscible. The mean value and degree of polydispersity of drop sizes have a significant effect on the key properties such as: stability [1,2]; viscosity and rheological behavior [3–5]; color and appearance [6]; texture [7]; and retention of aroma [8] and flavor (food emulsions) [9]. For this reason, many experimental techniques have been applied to determine the mean droplet size and the drop size distribution in emulsions, including microphotography and video-enhanced microscopy, gravitational/centrifugal sedimentation, Coulter counting, turbidimetry, differential scanning calorimetry, dynamic and static light scattering, acoustic spectroscopy and nuclear magnetic resonance (NMR). Excellent reviews on the characterization of emulsions with these and other methods have been compiled by Orr [10] and by several authors in the text of Sjöblom [11].

NMR-based methods offer significant advantages that distinguish them from the

other above-mentioned techniques [12]. The same sample can be tested as many times as desired. Dilution, cooling/heating, centrifugation or confinements in a narrow gap are not necessary. Measurements are not influenced by the optical or dielectric properties of the system. Therefore, clear and opaque emulsions, and dispersions in which the continuous phase is non-conducting can be tested. A typical test is fast (approx. 5–10 min), and it requires a small sample ($\geq \sim 0.5$ g). Furthermore, the composition of the emulsion can be resolved from the NMR data.

NMR microscopy on emulsions is based on the following few physical principles [13]: Some nuclei, such as protons (^1H), exhibit a permanent magnetic moment \mathbf{p} . When a steady uniform magnetic field \mathbf{B}_0 is applied on these nuclei, \mathbf{p} precesses around the direction of \mathbf{B}_0 at the Larmor frequency $\omega_0 = \gamma B_0$, where γ is a constant. Nuclei with precessing \mathbf{p} are termed spins. The ensemble of spins exhibit net magnetization \mathbf{M} in the direction of \mathbf{B}_0 . If a radio frequency (rf) pulse of a second magnetic field \mathbf{B}_1 orthogonal to \mathbf{B}_0 is applied, the net magnetization is rotated to an extent (typically 90 or 180°) that depends on the duration of the pulse. When the rf pulse ceases, \mathbf{M} will *relax* toward and eventually reach the equilibrium state. Relaxation of \mathbf{M} can be measured from the spins (protons) present in the emulsion, either in the direction of \mathbf{B}_0 (longitudinal magnetization), or transverse to it (transverse magnetization). In addition, the precession of spins at the same Larmor frequency is referred to as *coherent* or *in-phase*. If the steady magnetic field is not uniform as above the Larmor frequency depends on the position of the nuclei [$\omega(\mathbf{r}) = \gamma B(\mathbf{r})$]. Two spins at positions \mathbf{r}_1 and \mathbf{r}_2 , such that $\mathbf{B}(\mathbf{r}_1) \neq \mathbf{B}(\mathbf{r}_2)$, precess incoherently or out-of-phase. Magnetic field gradients are commonly applied to create a non-uniform steady magnetic field and adjust coherence.

Droplets in emulsions can be sized via NMR with at least two sequences of radio frequency and magnetic field gradient pulses: the echo train experiment introduced by Carr and Purcell [14] and refined by Meiboom and Gill (CPMG) [15], and the pulsed magnetic field gradient spin-echo experiment (PGSE) developed by Stejskal and Tanner [16]. This article describes classic views and novel contributions to the theory used to characterize emulsions from transverse magnetization data collected in these tests. The advantages and limitations of these methods are discussed. Furthermore, it is shown that a wealth of information on the emulsion besides the drop size distribution can be obtained when the results from both techniques are combined. The implementation of this combined CPMG–PGSE procedure is illustrated with the characterization of emulsions of water in several crude oils.

2. CPMG experiment: basic theory and interpretation

2.1. Description of the test

The CPMG sequence consists of a rf 90° pulse, followed by N rf 180° pulses that induce successive phase recoveries and generate a train of N spin-echoes (Fig. 1). As time proceeds, relaxation of the magnetization takes place and the amplitude of the spin-echo that is generated after each 180° re-phasing decays. In this experiment, the transverse component of the magnetization vector $M_{xy}(2n\tau)$ is

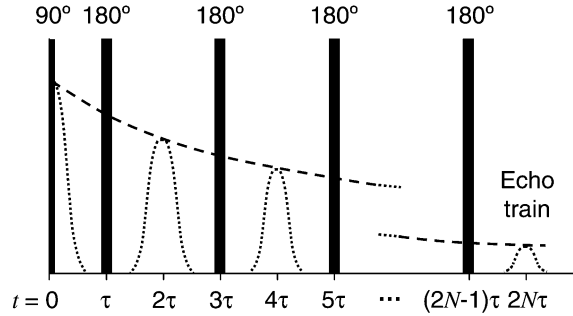


Fig. 1. Sequence of evens in a CPMG experiment.

measured, and the resulting relaxation curve is fitted to a discrete multi-exponential function of the form:

$$\frac{M_{xy}(2n\tau)}{M_{xy}(0)} = \sum_{i=1}^m f_i \exp\left(-\frac{2n\tau}{T_{2,i}}\right); \quad 0 \leq n \leq N; \quad m < N; \quad \sum_{i=1}^m f_i = 1, \quad (1)$$

$M_{xy}(0)$ is the amplitude of signal that corresponds to the initial transverse magnetization and f_i is the fraction of ^1H nuclei with characteristic relaxation time $T_{2,i}$. The fitting procedure consists of calculating f_i values for a pre-established set of $T_{2,i}$, whence the so-called T_2 distribution is obtained. Fitting data to a multi-exponential sum is an ill-posed problem, i.e. multiple sets of f_i values can render a satisfactory fit [17]. For this reason, a so-called regularization method must be implemented to calculate the most representative T_2 distribution [18].

2.2. Determination of drop sizes in emulsions via CPMG

Eq. (1) arises naturally when the relaxation of magnetization is modeled for an isotropic fluid confined in a planar, cylindrical or spherical cavity in the presence of volume-like and surface-like magnetization sinks with an average constant strength $1/T_{2,\text{bulk}}$ (*bulk relaxivity*) and ρ (*surface relaxivity*), respectively [19]. The contributions of bulk and surface relaxivity to the decay of transverse magnetization are accounted for in the $T_{2,i}$ values in the ‘fast diffusion’ mode as follows:

$$\frac{1}{T_{2,i}} = \frac{1}{T_{2,\text{bulk}}} + \rho \left(\frac{S}{V} \right)_i \quad (2)$$

$(S/V)_i$ is the surface-to-volume ratio of the cavity i . For a sphere of radius a_i , $(S/V)_i = 3/a_i$. Hence,

$$\frac{1}{T_{2,i}} = \frac{1}{T_{2,\text{bulk}}} + \rho \frac{3}{a_i} \quad (3)$$

and,

$$a_i = 3\rho \left(\frac{1}{T_{2,i}} - \frac{1}{T_{2,\text{bulk}}} \right)^{-1}. \quad (4)$$

The number of protons present in a given volume of sample determines the signal amplitude. For this reason, the fraction f_i that is associated to each $T_{2,i}$ value renders a direct measurement of the fraction of fluid that is confined in cavities of corresponding surface-to-volume ratio $(S/V)_i$. Therefore, the T_2 distribution that is obtained from isotropic fluids contained in the interstices of a heterogeneous system contains valuable information on the distribution of sizes of such heterogeneities. This principle is commonly used, for example, in the interpretation of lab and well logging T_2 measurements to estimate the size distribution of pores in rocks which potentially may contain hydrocarbons [20,21]. In a related application, the surface-to-volume ratio can be determined from independent measurements such as mercury porosimetry [22,23], pore image analysis [24] or BET gas adsorption [25,26] and the result is introduced in Eq. (2) to determine surface relaxivity at the rock-fluid interface.

Eq. (4) can be used to calculate the volume-weighted drop size distribution of emulsions containing spherical droplets, provided that:

- a. Measurements are performed in the ‘fast diffusion’ mode. This requirement is discussed in the next section.
- b. The surface relaxivity (ρ) and the bulk relaxivity ($1/T_{2,\text{bulk}}$) of the drop phase (water in *w/o* emulsions or vice versa) are known. $T_{2,\text{bulk}}$ can be easily measured from a CPMG experiment on a bulk sample of the drop phase, either in absence of continuous phase or in contact with it, but not emulsified. An independent measurement of the surface-to-volume ratio is required to calculate ρ .
- c. $T_{2,\text{bulk}}$ for the dispersed phase is indeed single-valued and not a distribution of characteristic bulk relaxation times.
- d. Two independent sets of $T_{2,i} - f_i$ values can be resolved from the T_2 distribution of the emulsion for the oil and water phases, respectively. This task is straightforward if the water signal and oil signal appear as separate peaks in the T_2 distribution. Otherwise, the magnetic resonance fluid method recently introduced by Freedman et al. [27] can be used to discriminate water signal from oil signal for systems in which the T_2 distributions of these phases overlap.

2.3. Range of drop sizes that can be resolved via CPMG

Eq. (4) is valid in the so-called fast diffusion limit (FDL), in which the characteristic timescale for diffusion of the molecules confined in the drops (t_D) is much smaller than the characteristic timescale for surface relaxation (t_ρ):

$$\frac{t_D}{t_\rho} = \frac{a_i^2/D}{a_i/\rho} \ll 1, \quad \text{whence} \quad \frac{\rho a_i}{D} \ll 1. \quad (5)$$

D is the self-diffusion coefficient of the drop phase. In practice, the relaxation of magnetization of fluids confined in spherical cavities occurs in the fast diffusion mode whenever:

$$\frac{\rho a_i}{D} \leq \frac{1}{4} \quad (6)$$

as shown in Appendix A. Therefore, the maximum diameter ($d_{\text{MAX,FDL}}$) for which Eq. (6) holds is

$$d_{\text{MAX,FDL}} = \frac{D}{2\rho}. \quad (7)$$

The signal-to-noise ratio (SNR) and the bulk relaxation time ($T_{2,\text{bulk}}$) can also determine d_{MAX} . The effect of surface relaxation on the decay of magnetization of fluid present in any droplet should be significantly greater than the intrinsic noise ν of the measurement. This condition can be expressed as follows:

$$\max[M_{xy}(t, a \rightarrow \infty) - M_{xy}(t, a)] \geq A\nu \quad (8)$$

where $A > 1$ is a constant. Eqs. (3), (8) and (56) in Appendix A can be combined to obtain,

$$\Delta M = A\nu; \quad \Delta M = M_{xy}(0) \exp\left(-\frac{t'}{T_{2,\text{bulk}}}\right) - M_{xy}(0) \exp\left(-\frac{t'}{T_{2,\text{bulk}}} - \frac{6\rho t'}{d_{\text{MAX},\nu}}\right), \quad (9)$$

where t' is the time at which ΔM exhibits a maximum and $d_{\text{MAX},\nu}$ is the maximum drop size that can be measured for given values of SNR and $T_{2,\text{bulk}}$.

Let the signal-to-noise ratio be defined as follows:

$$\text{SNR} = \frac{M_{xy}(0)}{\nu}. \quad (10)$$

It can be shown from Eqs. (9) and (10) that $t' = T_{2,\text{bulk}}$ when $\text{SNR} \gg A \exp(1)$. If so, the following expression for $d_{\text{MAX},\nu}$ is obtained:

$$d_{\text{MAX},\nu} = \frac{6}{A \exp(1)} \rho \text{SNR} T_{2,\text{bulk}}. \quad (11)$$

In summary, the maximum drop size that can be determined via CPMG is:

$$d_{\text{MAX}} = \min\{d_{\text{MAX,FDL}}, d_{\text{MAX},\nu}\} \quad (12)$$

where $d_{\text{MAX,FDL}}$ and $d_{\text{MAX},\nu}$ are given by Eqs. (7) and (11), respectively.

The self-diffusion coefficient of water at 25 °C is 2.30×10^{-9} m²/s [28] and a plausible surface relaxivity for oilfield emulsions is $\rho = 0.50$ $\mu\text{m/s}$ as shown later. For these conditions, water droplets up to $d_{\text{MAX,FDL}} = 2200$ μm could be sized according to Eq. (7). A typical signal-to-noise ratio for a CPMG experiment on emulsions is 250, and a plausible value for A is 3. In addition, $T_{2,\text{bulk}}$ for water at 25 °C is ca. 3 s. Therefore, from Eqs. (11) and (12) we obtain $d_{\text{MAX}} = d_{\text{MAX},\nu} = 276$ μm .

Eq. (12) restricts the T_2 values that can be considered to calculate the drop size distribution to an upper limit $T_{2,\text{MAX}}$:

$$\frac{1}{T_{2,\text{MAX}}} = \frac{1}{T_{2,\text{bulk}}} + \rho \frac{6}{d_{\text{MAX}}}. \quad (13)$$

We suggest to interpret the signal of the drop phase that is measured for $T_{2,i} > T_{2,\text{MAX}}$ as if it were originated from bulk fluid, and not from fluid dispersed in drops.

The minimum drop diameter (d_{MIN}) that can be measured via CPMG and its corresponding relaxation time $T_{2,\text{MIN}}$ are determined by the echo spacing. Let us assume that a fraction ε of the transverse component of magnetization of the fluid present in the smallest drops has relaxed when the first echo is acquired at time 2τ . If so,

$$1 - \varepsilon = \exp(-2\tau/T_{2,\text{MIN}}) \quad \text{whence } T_{2,\text{MIN}} \cong 2\tau/\varepsilon. \quad (14)$$

By substituting Eq. (14) in Eq. (4) we obtain:

$$d_{\text{MIN}} = 6\rho \left(\frac{\varepsilon}{2\tau} - \frac{1}{T_{2,\text{bulk}}} \right)^{-1} \cong \frac{12\tau\rho}{\varepsilon}. \quad (15)$$

The approximation that is made in Eq. (15) holds if $T_{2,\text{MIN}} \ll T_{2,\text{bulk}}$. A typical echo-spacing for a CPMG test is $2\tau = 300$ μs . If the surface relaxivity given above (0.5 $\mu\text{m/s}$) and $\varepsilon = 0.1$ are chosen, then $T_{2,\text{MIN}} = 3$ ms and $d_{\text{MIN}} = 9$ nm.

2.4. Determination of the water/oil composition in emulsions

The amplitude of the signal that is obtained from each phase is proportional to the number of protons present in such phase. Therefore, the volume fraction ϕ_k of phase k is related to the T_2 distribution as follows:

$$\phi_k \propto \frac{\sum (f_i)_k}{\text{HI}_k} \quad (16)$$

HI is the so-called hydrogen index, which is defined as the number of protons in a sample, divided by the number of protons present in the same volume of water [29]. Empirical correlations and diagrams to estimate HI are available for brines, and for light and heavy crude oils [30–32]. In general, $HI \sim 1.0$ for aqueous solutions and $HI \sim 0.9–1.0$ for most crude oils except for aromatic oils, which exhibit HI between 0.6 and 0.8 due to the low H/C ratio of aromatic compounds. If Eq. (16) holds, we have:

$$\phi_{DP} = \frac{\left[\sum (f_i)_{DP} / HI_{DP} \right]}{\left[\sum (f_i)_{CP} / HI_{CP} \right] + \left[\sum (f_i)_{DP} / HI_{DP} \right]}; \quad \phi_{CP} = 1 - \phi_{DP} \quad (17)$$

where the subindexes DP and CP identify the drop and continuous phase, respectively.

Low-field NMR-CPMG has been regarded as superior to all other available techniques for the determination of water content in heavy oil, bitumen and oilfield emulsions [33,34], and it is quickly becoming a standard procedure in the oil industry for such task. This application of the CPMG method has been discussed by LaTorraca et al. [29] and Hills [35]. Allsopp et al. [33] have developed and successfully tested in situ a low-field spectrometer suitable for usage in the field. The method was accurate to $\pm 5\%$ and measuring times were typically 4 min or less. This application is a natural extension of the usage of NMR relaxation measurements for the determination of porosity in minerals and rocks [20,24,26,36].

3. PGSE experiment: basic theory and interpretation

3.1. Description of the test

The pulsed field gradient spin-echo experiments consists of a rf 90° pulse, followed by a rf 180° pulse at time τ . As a result of this sequence, a spin-echo is collected at time 2τ (Fig. 2). The rf 180° pulse is sandwiched between two magnetic field gradient pulses of absolute strength g and duration δ that are separated by a time span Δ .

In a PGSE experiment, it is aimed to measure the amplitude of the spin-echoes in the presence and absence of gradient pulses ($g > 0$ and $g = 0$), respectively. In the latter case, the spin-echo is acquired in a homogeneous magnetic field and, therefore, $M_{xy}(2\tau, g=0, \Delta, \delta)$ is independent of the spatial distribution of spins in the sample. Conversely, when $g > 0$ the first gradient pulse imposes an inhomogeneous magnetic field, thus causing a loss of coherence in the phases of the spins to an extent that depends on the position of the nuclei at the time, the gradient is applied. In absence of diffusion, the second gradient pulse would exactly revert the phase shifts. However, since molecules diffuse and change their position during the *diffusion*

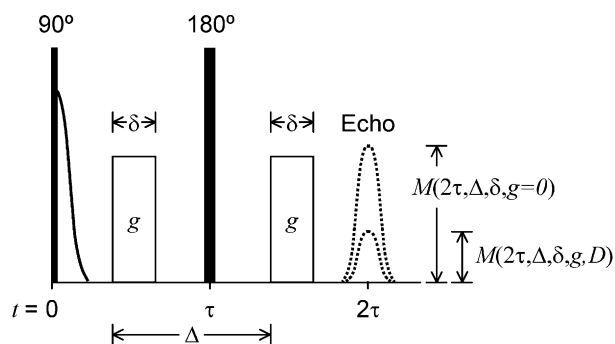


Fig. 2. Sequence of events in a PGSE experiment.

time Δ , the refocusing is incomplete and the amplitude of the echo that is recorded at time 2τ [$M_{xy}(2\tau, g > 0, \Delta, \delta, D)$] is smaller than $M_{xy}(2\tau, g = 0, \Delta, \delta)$. For this reason,

$$0 \leq M_{xy}(2\tau, g, \Delta, \delta, D) \leq M_{xy}(2\tau, g = 0, \Delta, \delta)$$

whence,

$$R = \frac{M_{xy}(2\tau, g, \Delta, \delta, D)}{M_{xy}(2\tau, g = 0, \Delta, \delta)}; \quad 0 \leq R \leq 1 \quad (18)$$

R is termed as the *spin-echo attenuation ratio*. In a typical PGSE experiment, attenuation ratios are measured by changing systematically δ , Δ or g .

For isotropic bulk fluids in which molecules can diffuse freely (Fickian diffusion), the following expression holds [16]:

$$R_{\text{bulk}} = \exp\left[-\gamma^2 g^2 D \delta^2 \left(\Delta - \frac{\delta}{3}\right)\right]. \quad (19)$$

The constant γ was mentioned earlier. It is called the gyromagnetic ratio of the nuclei ($\gamma = 2.67 \times 10^8 \text{ rad T}^{-1} \text{ s}^{-1}$ for ^1H). When Eq. (19) holds, a plot of the logarithm of R vs. $g^2 \delta^2 (\Delta - \delta/3)$ renders a straight line, and D can be calculated from the slope. This method is one of the very few experimental techniques available to measure self-diffusion coefficients.

3.2. Determination of drop sizes in emulsions via PGSE

Eq. (19) does not apply to fluids confined in small geometries such as pores or droplets, because molecules cannot diffuse freely. In this case, the dimensions of the cavity influence the loss of coherence in the phase of the spins when the

magnetic field gradient is applied, thus affecting the attenuation ratio R . Robertson [37] and Neuman [38] first proposed expressions for R for molecules confined between planes, within cylinders and spheres when a steady magnetic field gradient is applied. Murday and Cotts [39] extended Neuman's derivation for the PGSE sequence (Fig. 2), for restricted diffusion within a sphere of radius a . In this case, the attenuation ratio R_{sp} was shown to be given by:

$$R_{\text{sp}} = \exp\left\{-2\gamma^2 g^2 \sum_{m=1}^{\infty} \frac{1}{\alpha_m^2(\alpha_m^2 a^2 - 2)} \left[\frac{2\delta}{\alpha_m^2 D} - \frac{\Psi}{(\alpha_m^2 D)^2} \right]\right\}, \quad (20)$$

where,

$$\Psi = 2 + \exp[-\alpha_m^2 D(\Delta - \delta)] - 2 \exp(-\alpha_m^2 D\Delta) - 2 \exp(-\alpha_m^2 D\delta) + \exp[-\alpha_m^2 D(\Delta + \delta)], \quad (21)$$

α_m is the m th positive root of the equation:

$$\alpha a J_{5/2}(\alpha a) - J_{3/2}(\alpha a) = 0 \quad (22)$$

and J_k is the Bessel function of the first kind, order k .

Two limiting cases of Eq. (20) are of interest. First, for very large spheres ($a \rightarrow \infty$), Eq. (20) reduces to Eq. (19) [$R_{\text{sp}}(a \rightarrow \infty) = R_{\text{bulk}}$] as might be expected, because the effect of restricted diffusion on R becomes negligible. Second, for very small spheres ($a \rightarrow 0$), Eq. (20) simplifies as follows:

$$R_{\text{sp}}(a \rightarrow 0) = 1 - \frac{16}{175} \gamma^2 g^2 D^{-1} \delta a^4 \rightarrow 1. \quad (23)$$

The probability of the molecules to displace during the diffusion time Δ is reduced as $a \rightarrow 0$. For this reason, the loss of coherence in the phases of the spins caused by the magnetic field gradient diminishes and less attenuation of the spin-echo is observed, whence $R \rightarrow 1$ as predicted by Eq. (23).

In the derivation of Eq. (20), it is assumed that the phase shifts of spins diffusing in a bounded region exhibit a normal (Gaussian) distribution. However, this so-called Gaussian phase-distribution (GPD) approximation is exact only for spins undergoing free diffusion [38]. Balinov et al. [40] performed Brownian dynamics simulations for restricted diffusion in spheres of selected sizes at fixed g , Δ and for various δ , to calculate the exact attenuation ratio that would be observed in each case. Least-square fits of these results were performed using Eq. (20) and the sphere radius a as fitting parameter. The radii calculated with this expression differed by less than 5% from the sizes set for the simulations. Whence, it was concluded that the GPD approximation and Eq. (20) are adequate to account for the decay of transverse magnetization of fluids confined in spheres.

For emulsion with a finite distribution of (spherical) droplet sizes, Packer and Rees [41] first proposed that the attenuation ratio of the drop phase (R_{DP}) can be calculated as the sum of the attenuation ratios $R_{sp}(a)$ that would be recorded for fluid confined in drops of radii a , weighted by the probability of finding drops with such sizes in the dispersion. This is:

$$R_{DP} = \int_0^{\infty} p_V(a) R_{sp}(a) da / \int_0^{\infty} p_V(a) da \quad (24)$$

where $p_V(a)$ is the volume-weighted distribution of sizes. $R_{sp}(a)$ is determined from Eq. (20). The task of determining $p_V(a)$ from the PGSE data is feasible, but requires a large number of measurements of R for which the duration of the test may become impractical as discussed later. Instead, a few data are usually taken and an empirical form of $p_V(a)$ is assumed. The lognormal probability distribution function (p.d.f.),

$$p_V(a) = \frac{1}{2a\sigma(2\pi)^{1/2}} \exp\left\{-\left[\frac{\ln(2a) - \ln(d_{gV})}{2\sigma^2}\right]^2\right\} \quad (25)$$

is the classic assumption for the drop size distribution in absence of additional information, because it is well known that sequential break-up processes, such as grinding of solids or disruption of droplets under mechanical agitation, lead to a lognormal distribution of particle and drop sizes, respectively [42,43]. In Eq. (25), d_{gV} and σ are the geometric volume-based mean diameter and the width or geometric standard deviation of the distribution, respectively. The determination of the drop size distribution consists of performing a least-square fit of the experimental data for R with Eqs. (24) and (25), using d_{gV} and σ as fitting parameters.

In the original work of Packer and Rees and most of the subsequent publications about this method [12,44–52], Eqs. (24) and (25) are expressed in terms of the number-based drop size distribution $p_N(a)$. It can be shown that if $p_V(a)$ is lognormal with characteristic parameters d_{gV} and σ , the corresponding number-based distribution $p_N(a)$ is also lognormal with the same geometric standard deviation σ and number-based mean size $d_{gN} = d_{gV} \exp(-3\sigma^2)$ [53]. Although both approaches are numerically equivalent, it is more proper to express these equations in terms of the volume-weighted distribution because the amplitude of transverse magnetization that is measured in a PGSE test is proportional to the volume of liquid present in the system as drops, and not to the number of droplets.

Packer and Rees [41] correctly pointed out that their procedure is useful to determine the drop size distribution when the following assumptions are valid:

- a. The spin-echo is originated solely from only one component of the emulsion, i.e. the drop phase. Therefore,

$$R_{EMUL} = R_{DP}. \quad (26)$$

This assumption limits the applicability of the method to emulsions for which the signal from the continuous phase is suppressed (i.e. emulsions of oil in D₂O). Eq. (26) also applies if the transverse magnetization of the continuous phase has relaxed completely and the natural (bulk) relaxation of the drop phase is small at the time the spin-echo is acquired. Namely,

$$(T_{2,\text{bulk}})_{\text{CP}} \ll 2\tau \ll (T_{2,\text{bulk}})_{\text{DP}} \quad (27)$$

where $(T_{2,\text{bulk}})_{\text{CP}}$ and $(T_{2,\text{bulk}})_{\text{DP}}$ are the characteristic bulk relaxation times of the continuous and drop phases, respectively. Emulsions of water in viscous oils often satisfy Eq. (27). This explains why the PGSE method is commonly applied in the determination of drop sizes in margarine, butter and low-calorie spreads [44,46,47,49,54] and water-in-crude-oil emulsions [45].

- b. The distribution of drop sizes is indeed lognormal. This is a significant shortcoming of the method, because the shape of the distribution is not resolved independently, but assumed a priori. Drop sizes are often, but not always, distributed in a lognormal fashion [53] and, therefore, Eq. (25) does not provide a satisfactory fit of the PGSE data in all cases [50,54,55].
- c. The effect of surface relaxation on the amplitude of the spin-echo is negligible. In the derivation of Eq. (20), Murday and Cotts assumed $\rho=0$. For this reason, surface relaxation is not accounted for in the Packer–Rees method. It can be anticipated that this effect is indeed negligible in a PGSE experiment performed in the fast diffusion regime, because in such regime the relaxation due to diffusion of the spins is much more significant than surface relaxation ($1/t_D \gg 1/t_p$ whence $\rho a/D \ll 1$, see Eq. (5)).

Dunn and Sun [34] considered the effect of surface relaxation on the attenuation ratio R_{sp} by changing the boundary condition in Neuman's and Murday and Cotts' derivation for the solution of the diffusion propagator of the spins P (see Eq. (11) in Neuman's paper) from:

$$D\nabla P|_{r=a} = 0 \quad (28)$$

to:

$$D\nabla P + \rho P|_{r=a} = 0 \quad (29)$$

to obtain:

$$R_{\text{sp},\rho} = \exp\left\{-2\gamma^2 g^2 \sum_{m=1}^{\infty} \frac{1}{\alpha_m^2 (\alpha_m^2 a^2 - 2 + \rho^2 a^2 / D^2 - \rho a / D)} \left[\frac{2\delta}{\alpha_m^2 D} - \frac{\Psi}{(\alpha_m^2 D)^2} \right]\right\}, \quad (30)$$

where Ψ is given by Eq. (21) as before and α_m is the m th positive root of the equation:

$$\alpha a J_{5/2}(\alpha a) - \left(1 + \frac{\rho a}{D}\right) J_{3/2}(\alpha a) = 0. \quad (31)$$

Eq. (30) applies only for small ρ and large D so the probability of finding a spin anywhere in the drop is nearly uniform and the GPD approximation is satisfied (see discussion after Eq. (23)). Otherwise, significant surface relaxation would take place and a non-Gaussian distribution of the phase shifts of the spins near the water/oil interfaces would be observed. Eq. (30) reduces to Eq. (20) in the limit $\rho a/D \rightarrow 0$, as might be expected.

The PGSE experiment has been used not only to size drops in emulsions as discussed above, but also pores in mineral samples [56–58], biological cells [16,56,59] and heterogeneities in organic tissue [60,61]. The three-dimensional packing of non-spherical drops in highly concentrated emulsions ($\phi_{DP} \sim 1$) has also been studied with this method [62,63]. Other applications in connection with emulsions include the characterization of micelles, bicontinuous structures in microemulsions, vesicles and liquid crystals in surfactant/oil/water systems [47,64–67].

Several modifications of the basic PGSE sequence shown in Fig. 2 have been proposed and used in emulsion studies. The stimulated spin-echo (SSE) [68] and the longitudinal-eddy-current-delay (LED) [69] modification allow better resolution for systems exhibiting significantly different longitudinal and transverse relaxation times. The flow-compensating PGSE [51] is used to characterize emulsions in laminar flow. The interpretation of the spin-echo attenuation of the drop phase via Eqs. (20)–(25) also holds for these sequences.

3.3. A novel theory to resolve PGSE data in the time domain

The first limitation listed above for the PGSE test, namely the impossibility to resolve for the drop size distribution when the contribution of the magnetization of the continuous phase to the spin-echo is significant, was overcome with the introduction of the Fourier-transform PGSE method (FT-PGSE). Excellent reviews on this method and its applications in the characterization of water/oil/surfactant systems have been published by Stilbs [70] and Söderman and Stilbs [71]. In the FT-PGSE procedure, the second half of the spin-echo that is generated in the PGSE sequence is Fourier-transformed, and the individual contributions of the components to the spin-echo appear as separate peaks in the frequency domain due to differences in chemical shift. Lönnqvist et al. [52] applied this technique to resolve for the individual signal of water and oil in simple (w/o) and multiple ($w/o/w$) emulsions. Ambrosone et al. [54] used the method to isolate the water signal from margarine and emulsions of water in olive oil.

Better resolution of the Fourier spectrum is attained as the strength of the permanent magnetic field is increased. For this reason, high-field magnets with

Larmor frequencies typically above 80 MHz are used in FT-PGSE studies. Unfortunately, individual peaks cannot be resolved satisfactorily at the frequencies at which low-field NMR spectrometers operate (approx. 2 MHz). Therefore, the determination of the individual contributions of water and oil to the spin-echo that is obtained from an emulsion in the time domain is relevant. The following theoretical framework aims to address this matter. Details on the derivation of the equations are provided in Appendix A.

We propose that the attenuation ratio of emulsions should be computed as follows:

$$R_{\text{EMUL}} = (1 - \kappa)R_{\text{DP}} + \kappa R_{\text{CP}}; \quad 0 \leq \kappa \leq 1, \quad (32)$$

where R_{DP} and R_{CP} are the time-resolved attenuation ratios of the drop and continuous phases, respectively. κ is a parameter associated to the natural relaxation of the transverse component of the magnetization of both phases. It is shown in Appendix A that for the basic PGSE sequence (Fig. 2), κ is given by:

$$\begin{aligned} \kappa &= \left[1 + \frac{\sum (f_i)_{\text{DP}} \exp[-2\tau/(T_{2,i})_{\text{DP}}]}{\sum (f_i)_{\text{CP}} \exp[-2\tau/(T_{2,i})_{\text{CP}}]} \right]^{-1} \\ &\cong \left[1 + \frac{\phi_{\text{DP}} \text{HI}_{\text{DP}} \exp[-2\tau/(T_{2,\text{bulk}})_{\text{DP}}^*]}{\phi_{\text{CP}} \text{HI}_{\text{CP}} \sum (x_i)_{\text{CP}}^* \exp[-2\tau/(T_{2,i})_{\text{CP}}^*]} \right]^{-1}; \quad (x_i)_{\text{CP}}^* = \frac{(f_i)_{\text{CP}}^*}{\sum_j (f_j)_{\text{CP}}^*}, \end{aligned} \quad (33)$$

where the $T_{2,i} - f_i$ values for each phase in the exact expression are determined from the T_2 distribution of the emulsion via CPMG as explained above. The approximation shown in Eq. (33) allows the evaluation of κ from the T_2 distribution of the phases tested independently or in contact as bulk fluids [parameters noted with (*)]. It is also implied in the approximation that the drop phase exhibits a single characteristic relaxation time, whereas the continuous phase is allowed to exhibit a distribution of relaxation times.

The emulsions that can be characterized with the Packer–Rees approach fall within the particular cases of this derivation. When the signal of the continuous phase is suppressed, or it has relaxed completely at the time the spin-echo is acquired, $\kappa \rightarrow 0$ according to Eq. (33). Therefore, Eq. (32) reduces to Eq. (26). On the other hand, $\kappa \rightarrow 1$ corresponds to the case in which the amplitude of the spin-echo is determined solely by the continuous phase. These limiting cases are discussed in Appendix A.

R_{DP} in Eq. (32) is given by Eq. (24) as before. $R_{\text{sp}}(a)$ is calculated using Eq. (20). Eq. (30) can be used instead of Eq. (20) if it is desired to consider the effect of ρ on $R_{\text{sp}}(a)$. Eqs. (20) and (30) are compared quantitatively in Section 7.6.

For the general case in which the continuous phase exhibits a distribution of diffusion coefficients p_D that is either known or determined independently, R_{CP} can

be calculated according to:

$$R_{\text{CP}} = \int_0^\infty p_D(D_{\text{CP}}) R_{\text{bulk,CP}}(D_{\text{CP}}) dD_{\text{CP}} / \int_0^\infty p_D(D_{\text{CP}}) dD_{\text{CP}}. \quad (34)$$

For diluted emulsions ($\phi_{\text{DP}} \ll 1$), it can be assumed that the spins diffuse freely, whence $R_{\text{bulk,CP}}$ is given by Eq. (19). As the volume fraction of the drop phase increases, droplets restrict the diffusion paths of the spins in the continuous phase [72]. This effect is commonly accounted for by defining an obstruction factor ζ as the ratio between the measured (effective) self-diffusion coefficient $D_{\text{CP,eff}}$ and its actual value D_{CP} . For diffusion restricted by spheres of uniform size, Jönsson et al. [73] showed that:

$$\zeta = \frac{D_{\text{CP,eff}}}{D_{\text{CP}}} = \frac{1}{1 + \frac{1}{2}\phi_{\text{DP}}}. \quad (35)$$

This expression holds independently of the spatial arrangement of the spheres up to $\phi_{\text{DP}} \sim 0.30$ [74,75]. ζ has been computed in simulations of self-diffusion in a fcc lattice of spheres [75]. We have correlated such results with the following empirical equation:

$$\zeta = \frac{1}{1 + \frac{1}{2}\phi_{\text{DP}} + \frac{1}{4}(\phi_{\text{DP}}/\phi_{\text{MAX,fcc}})^9}; \quad \phi_{\text{DP}} < \phi_{\text{MAX,fcc}} \quad (36)$$

where $\phi_{\text{MAX,fcc}} = \sqrt{2}\pi/6 \cong 0.7405$ is the volume fraction at which droplets reach close-packing. Analogous expressions to Eq. (36) can be derived for sc and bcc lattices from the data reported in Refs. [74,75].

The effect of restricted diffusion on R_{CP} is taken into account by replacing $p_D(D)$ with $p_{\zeta D}(D)$ in Eq. (34), and computing ζ from Eq. (36). This approach is exact for regularly arranged, monodisperse drops, but approximate for irregularly arranged, polydisperse ones. In any case, Jönsson et al. [73] showed that the minimum value of ζ is obtained for diffusion amidst regularly arranged spheres, and that it increases only moderately for random arrangements. According to their model, polydispersity would not affect ζ in systems with moderate concentration of droplets ($\phi_{\text{DP}} \sim < 0.20$).

3.4. Range of drop sizes that can be resolved via PGSE

The maximum drop size that can be determined via PGSE is related to the one-dimension root-mean-square displacement of spins undergoing free (Fickian) self-

diffusion in isotropic, isothermal media during the diffusion time Δ :

$$d_{\text{MAX}} \approx \sqrt{2} \langle x^2 \rangle^{1/2} = \sqrt{2} \left\{ \int_{-\infty}^{\infty} (x-x_0)^2 \frac{\exp[-(x-x_0)^2/4D_{\text{DP}}t]}{\sqrt{4\pi D_{\text{DP}}t}} dx \Big|_{t=\Delta} \right\}^{1/2} \\ = 2\sqrt{D_{\text{DP}}\Delta}. \quad (37)$$

Most of the molecules confined in a droplet with diameter much larger than d_{MAX} would not ‘feel’ any restriction in their diffusion path due to the presence of the water/oil interface. For this reason, such drop would not be sized accurately. This expression for d_{MAX} is also obtained by requiring the characteristic diffusion time in the drops with size d_{MAX} to be comparable to Δ ($t_{D,\text{MAX}} = a_{\text{MAX}}^2/D_{\text{DP}} \approx \Delta$). The factor $\sqrt{2}$ has been included in Eq. (37) to assure consistency between these two approaches.

Eq. (37) suggests that d_{MAX} can be increased at will with Δ . However, the diffusion time must be adjusted keeping in mind that $\Delta < (T_{2,\text{bulk}})_{\text{DP}}$. Otherwise, the data will be affected by natural (bulk) and surface relaxation of the magnetization and, therefore, by a reduction in the signal-to-noise ratio.

Low self-diffusivities render small values for d_{MAX} . In addition, low-mobility molecules usually exhibit short relaxation times [27] and, therefore, short values of Δ must be chosen in such cases. In general, it is not possible to determine droplet sizes via PGSE for drop phases exhibiting self-diffusion coefficients below 10^{-12} m²/s [12].

An expression for the minimum drop size d_{MIN} that are measurable from PGSE data can be obtained from Eq. (23):

$$d_{\text{MIN}} = \left(175\lambda \frac{D_{\text{DP}}}{\gamma^2 g^2 \delta_{\text{MAX}}} \right)^{1/4},$$

where $\lambda = 1 - R_{\text{sp}}(a = d_{\text{MIN}}/2)$, $\delta = \delta_{\text{MAX}}$ and δ_{MAX} is the maximum duration that is chosen for the magnetic field gradient pulse. In all cases δ must be smaller than Δ . Otherwise, the first pulsed gradient would overlap with the 180° rf pulse (see Fig. 2). In order to avoid such problem we suggest choosing $\delta_{\text{MAX}} = \Delta/3$ and $\tau = \Delta$ for experiments performed varying δ at constant Δ and g . With this definition of δ_{MAX} , the expression given above becomes:

$$d_{\text{MIN}} = \left(525\lambda \frac{D_{\text{DP}}}{\gamma^2 g^2 \Delta} \right)^{1/4}. \quad (38)$$

It was shown via Eq. (23) that $R_{\text{sp}}(a \rightarrow 0) \rightarrow 1$. Therefore, the reduction in the attenuation ratio λ when $a = d_{\text{MIN}}/2$ is small ($0 < \lambda \ll 1$), yet it must be measurable in order to resolve for d_{MIN} . Plausible values for λ are $0.05 \leq \lambda \leq 0.01$.

The usefulness of Eqs. (37) and (38) can be illustrated with typical conditions

for a PGSE test on *w/o* emulsions, for which $D_{DP}=2.30\times 10^{-9}$ m²/s ($T=25$ °C); $\Delta=200$ ms; $g=0.25$ T/m. For this example, the attenuation ratio is sensitive to drop sizes between $d_{MIN}=1$ μm ($\lambda=0.01$) and $d_{MAX}=42$ μm , according to Eqs. (38) and (37), respectively. These calculations agree with the assessment of Balinov et al. [12], who pointed out that the PGSE method allows resolution of droplet sizes between 1 and 50 μm when $g\sim 1$ T/m. It is worth emphasizing that Eqs. (37) and (38) can be used to calculate d_{MIN} and d_{MAX} for arbitrary sets of PGSE parameters.

4. Combined CPMG-PGSE method

4.1. Advantages and limitations of the CPMG experiment

The main advantage of the CPMG method is that thousands of spin-echoes are acquired in one test. From the large dataset that is obtained in this experiment, drop size distributions with arbitrary shape can be determined. The calculations reported above suggest that the method can resolve drop sizes ranging from approximately 0.01 to approximately 300 μm . In addition, the water/oil composition of the emulsion can be calculated. A CPMG test typically takes about 5 min to be completed, as reported later. The short duration of the test makes it suitable to keep track of the stability of the emulsion and of rapid changes in the drop size distribution. Finally, the CPMG test is independent of the self-diffusivity of the phases because it is performed in absence of magnetic field gradients. Therefore, the T_2 distribution of the emulsion can be fully interpreted in terms of bulk and surface relaxation. However, the surface relaxivity cannot be determined from CPMG. An independent measurement of the surface-to-volume ratio is required to evaluate ρ .

4.2. Advantages and limitations of the PGSE experiment

In the PGSE method, the contributions of the water and oil phases can be resolved independently in the frequency domain with a high-field spectrometer if the FT-PGSE technique is applied, or in the time domain with the theoretical framework introduced in this article. Also, in the fast diffusion regime the attenuation ratio is not affected by surface relaxation and, therefore, the PGSE data can be interpreted solely in terms of self-diffusivity and bulk relaxation. As a result, an independent measurement of the drop size distribution and, therefore, of the surface-to-volume ratio of the drop phase in the emulsion, can be performed with this procedure.

Nevertheless, the PGSE method is very slow: acquiring a dataset comparable to that of a single CPMG test would take several days. For this reason, in a typical PGSE experiment only a few (approx. 10–20) attenuation ratios are measured in 5–20 min. Due to lack of data, the drop size distribution is resolved assuming in advance a p.d.f. to describe it. Finally, the range of drop sizes that can be determined precisely with this method is narrow (approx. 1–50 μm).

4.3. Combining experimental data from both methods

The shortcomings of the two methods can be overcome, and their advantages integrated, by combining data from both experiments. In the proposed approach, a CPMG test followed by a typical PGSE experiment as described above are performed on the same emulsion sample and the data are processed as follows:

- a. The T_2 distribution of the emulsion is determined from the transverse relaxation (CPMG) dataset using Eq. (1) and a suitable regularization method [17]. The water/oil composition is calculated from Eq. (17). The parameter κ is determined using Eq. (33).
- b. An initial value is assumed for the surface relaxivity.
- c. The volume-weighted drop size distribution is determined from the T_2 distribution of the drop phase via Eq. (4). The corresponding cumulative distribution $P_{V,EXP}(a_i)$ is calculated as:

$$P_{V,EXP}(a_i) = \frac{\sum_{j=1}^i (f_j)_{DP}}{\sum_{j=1}^m (f_j)_{DP}} \quad 1 \leq i \leq m. \quad (39)$$

- d. The cumulative distribution of sizes is fitted (least-square analysis) with a modified form of the bimodal Weibull cumulative probability distribution function [76],

$$P_V(a) = \begin{cases} 0 & a < a_0 \\ \omega \left\{ 1 - \exp \left[- \left(\frac{u}{\sigma_1} \right)^{m_1} \right] \right\} + (1 - \omega) \left\{ 1 - \exp \left[- \left(\frac{u}{\sigma_2} \right)^{m_2} \right] \right\}; & u = \ln \frac{a}{a_0}; a > a_0 \end{cases} \quad (40)$$

where $0 \leq \omega \leq 1$; $m_1, m_2 > 0$; $\sigma_1, \sigma_2 > 0$ are adjustable parameters and a_0 is the smallest drop size a_i calculated from the T_2 distribution of the drop phase such that $f_i = 0$ and $f_{i+1} > 0$. The set of parameters that are determined with this procedure defines the volume-based drop size distribution $p_V(a)$, which is given by:

$$p_V(a) = \frac{dP_V(a)}{da} = \begin{cases} 0 & a < a_0 \\ \frac{1}{a} \left\{ \frac{\omega m_1}{\sigma_1^{m_1}} u^{m_1-1} \exp \left[- \left(\frac{u}{\sigma_1} \right)^{m_1} \right] + \frac{(1 - \omega) m_2}{\sigma_2^{m_2}} u^{m_2-1} \exp \left[- \left(\frac{u}{\sigma_2} \right)^{m_2} \right] \right\} & a > a_0 \end{cases} \quad (41)$$

This p.d.f. has been chosen because it can fit unimodal and bimodal, symmetric, left-skewed and right-skewed distributions. However, if the experimental drop size distribution is unimodal and log-symmetric, the fit can be performed with the cumulative form of the lognormal distribution:

$$P_V(a) = \frac{1}{2} \left[1 + \operatorname{erf} \left(\frac{\ln(2a) - \ln(d_{gV})}{\sqrt{2}\sigma} \right) \right] \quad (42)$$

where $\operatorname{erf}(z) = \frac{2}{\sqrt{\pi}} \int_0^z e^{-t^2} dt$ is the error function.

- e. To calculate the attenuation ratios of the drop phase R_{DP} , the distribution $p_V(a)$ is substituted into Eq. (24) along with a suitable expression for $R_{sp}(a)$ [Eq. (20)]. The same set of parameter δ , Δ and g chosen for the PGSE experiment must be used in the calculations. R_{CP} is calculated using Eq. (34). R_{EMUL} is calculated from Eq. (32).
- f. The value of ρ is adjusted in successive iterations, and the procedure repeated until:

$$\min\{\chi^2(\rho)\} = \min\left\{ \sum_{j=1}^l [(R_{EMUL,EXP})_j - (R_{EMUL})_j]^2 \right\} \quad (43)$$

is attained. $R_{EMUL,EXP}$ stands for the set of l experimental attenuation ratios acquired in the PGSE test.

5. Computational procedures

The T_2 distributions were calculated from CPMG relaxation data with codes developed by Huang [77] in Matlab (The MathWorks, Inc.) and FORTRAN. The calculation of κ , and the least-square analysis referred to above were performed with a Matlab program. Excel spreadsheets (Microsoft) were also developed to verify numerical results.

The multidimensional downhill simplex method was chosen to perform least-square minimization in steps (d) and (f) of Section 4.3. Code published in the text of Press et al. [78] was adapted for this task. The following arbitrary definitions were made for the determination of the parameters of the Weibull distribution:

$$m_1 = \Lambda_1^2; \quad m_2 = \Lambda_2^2; \quad \sigma_1 = \Lambda_3^2; \quad \sigma_2 = \Lambda_4^2; \quad \omega = [1 + \exp(-\Lambda_5)]^{-1} \quad (44)$$

and the minimization of the error was performed adjusting the values of Λ_1 through Λ_5 . The definitions given in Eq. (44) make the fitting parameters unbounded ($-\infty < \{\Lambda_1, \Lambda_2, \Lambda_3, \Lambda_4, \Lambda_5\} < \infty$) and avoid constrains for the reflections of the simplex.

The integrals depicted in Eq. (24) were solved numerically using 24-point Gauss integration [79]. This method requires modifying the integration range from $(0, \infty)$ to $(-1, 1)$. For the Weibull distribution, this is achieved with negligible error via the following change of variables:

$$u_{\text{WD}} = 2 \frac{\ln a - \ln a_0}{\ln a_N - \ln a_0} - 1 \quad (45)$$

where a_N is the largest drop size of the experimental drop size distribution for which $f_N = 0$ and $f_{N-1} > 0$. If the lognormal distribution (Eq. (25)) is used instead to describe $p_V(a)$, integration is performed in terms of u_{LND} ,

$$u_{\text{LND}} = \frac{a^{1/\sigma} - (d_{gV}/2)^{1/\sigma}}{a^{1/\sigma} + (d_{gV}/2)^{1/\sigma}}. \quad (46)$$

We have found that using Eq. (46) instead of the definition for u_{LND} suggested by Söderman et al. [47] [$u_{\text{LND}} = (a - d_{gV}/2)/(a + d_{gV}/2)$], reduces the error made with numerical integrations in the calculation of R_{DP} , particularly for narrow drop size distributions.

Forty sets of synthetic transverse relaxation and restricted diffusion data were generated at varying signal-to-noise ratio. These data were further used to evaluate the convergence characteristics of the code. Convergence to the expected solution was achieved in all cases. The difference between calculated and actual values of the parameters was in proportion to the noise level imposed to the signal. The time needed for convergence of the two annealed simplex minimizations was typically 15 s in a computer equipped with a 750 MHz processor.

6. Experimental

Synthetic water-in-crude-oil emulsions were made with distilled water dispersed in three crude oils, further referred to as Rice-1, Rice-2 and Rice-3. The properties and composition of the oils are described in Table 1. Indigenous materials present in the oils, such as asphaltenes and resins, sufficed to stabilize the emulsions.

The NMR measurements were performed using a MARAN II Spectrometer (2.2 MHz, Resonance Inc.). A thermocouple placed in the center of the samples after each test consistently reported 25.5 ± 0.5 °C. In the CPMG experiments, the echo spacing was 315 μs , the number of echoes was 12 288. PGSE parameters are indicated for each test in Section 7. CPMG and PGSE experiments were performed on 10-ml samples of water and crude oils, placed in plastic cylindrical containers (1 inch ID) to determine hydrogen indexes and distribution of diffusion coefficients in the oils as discussed later.

Water/oil mixtures and emulsion samples of 20 ml were prepared as follows: the water and oil phases were poured carefully in the containers to prevent emulsification, and left in contact during 24 h. When the formation of emulsions was sought,

Table 1
Properties and composition of the crude oils used in this study

Property/Component	Units	Rice-1	Rice-2	Rice-3
°API		28.5	28.7	20.5
Shear viscosity ^a	mPa s	27	33	207
Relaxation time ($T_{2,\text{bulk}}$)	ms	91	57	8.7
Hydrogen index		0.986	0.928	0.906
Self-diffusion coefficients				
D_{LM}	m ² /s	1.78×10^{-10}	1.75×10^{-10}	7.3×10^{-12}
σ_D		0.27	0.75	–
SARA analysis ^b				
Saturates	wt.%	51.82	32.48	30.8
Aromatics	wt.%	37.67	50.90	20.5
Resins	wt.%	7.53 (4.67)	14.28 (9.19)	31.6 (29.2)
Asphaltenes	wt.%	2.97 (1.84)	2.34 (1.50)	17.1 (15.8)
% Loss in evaporation	wt.%	38.0	35.7	7.7
Element analysis ^c				
Aluminum (Al)	ppm	<0.2	0.5	0.3
Barium (Ba)	ppm	<0.02	0.05	0.04
Calcium (Ca)	ppm	1.2	4.40	51
Chromium (Cr)	ppm	0.07	0.05	0.04
Cobalt (Co)	ppm	0.10	0.40	0.04
Copper (Cu)	ppm	<0.02	0.16	0.13
Iron (Fe)	ppm	2.4	7.9	51
Magnesium (Mg)	ppm	0.4	0.40	4.4
Manganese (Mn)	ppm	<0.02	<0.02	1.9
Molybdenum (Mo)	ppm	<0.20	<0.2	<0.2
Nickel (Ni)	ppm	1.0	13	2.9
Potassium (K)	ppm	<0.2	2.1	1.7
Sodium (Na)	ppm	1.8	3.5	6.4
Strontium (Sr)	ppm	<0.02	<0.02	<0.02
Vanadium (V)	ppm	0.14	33	0.11
Zinc (Zn)	ppm	0.36	1.2	40

^a Shear viscosity measured at 30 °C and shear rate of 1 s⁻¹.

^b Composition of oil topped at 60 °C with N₂ stream. Numbers in parenthesis stand for composition of oil as received (before topping). For example, in the composition of the crude oil Rice-1, 1.84 = $2.97 \times (1 - 38.0/100)$. Tests performed by Baseline DGSI–Analytical Laboratories.

^c Element analyses performed by OndeoNalco Energy Services, L.P.

the phases were dispersed with a rectangular paddle (0.8 inch × 0.4 inch) placed at the tip of a rod connected to a rotating device. Each sample was stirred at 750 rev./min for 10 min. Some samples were ultrasonicated (Branson sonifier 450) to further reduce the drop sizes.

Drop size distributions of selected emulsions were also determined via microphotography. The procedure required pre-treating 0.4 × 4 × 40 mm glass cells via chemical reaction with octadecyltrichlorosilane (Sigma) to make their surfaces hydrophobic and thus avoid spreading of water droplets [80]. Since the emulsions were not transparent, they were diluted with toluene to allow observation under the

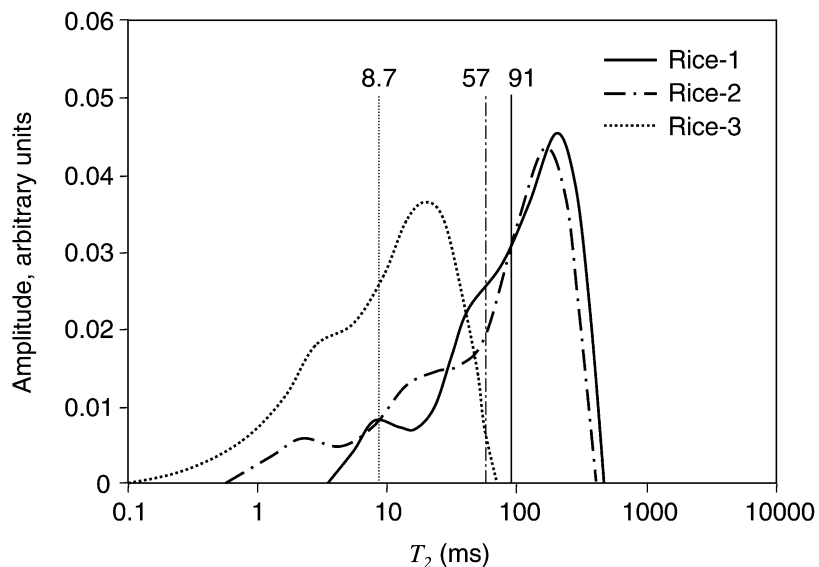


Fig. 3. T_2 distributions of the crude oils used in this study.

microscope. Digital pictures were taken with $20\times$ and $40\times$ objectives at different levels throughout the 0.4-mm gap with a Nikon Eclipse TE300 microscope connected to a Kodak Ekta Pro motion analyzer, model 1000 HRC, and images were further processed with a kit of macros for Adobe Photoshop. In all cases, 1063 droplets were randomly chosen and their sizes measured. This number assures statistical significance of 5% error with 99% confidence for the resulting drop size distribution [81].

7. Results and discussion

7.1. Properties of the pure fluids

Fig. 3 summarizes CPMG results for the T_2 distributions of the oils used in these experiments, along with their corresponding logarithmic mean. In all cases, broad distributions of relaxation times were obtained.

Low relaxation times are typically observed at high viscosity/temperature ratios and vice versa [82]. This explains why Rice-3, which had the highest shear viscosity (Table 1) relaxed, in average, faster than Rice-1 and Rice-2. Rice-1 and Rice-2 oils had nearly the same viscosity, yet the ratio of the $T_{2,LM}$ values (Rice-1:Rice-2) was 1.6:1. Table 1 shows that Rice-2 contained more aromatics and resins than Rice-1, and also a higher concentration of paramagnetic materials such as Fe and V. Aromatic compounds exhibit shorter T_2 values than alkanes with similar carbon number. Macromolecules with aromatic rings such as asphaltenes and resins also exhibit short relaxation times, in the order of 0.1–5 ms. Also, paramagnetic materials

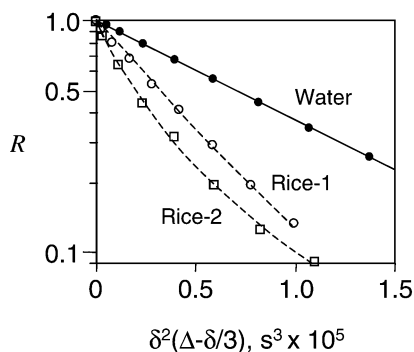


Fig. 4. PGSE data for water and crude oils Rice-1 and Rice-2. The values of g , Δ and δ used in each test are reported in the text.

generate inhomogeneities in the steady magnetic field that lead to faster relaxation of the magnetization. These facts may explain the referred difference in T_2 . Finally, a CPMG test was also performed on a sample of pure water. In this case, the decay of magnetization could be described with a single relaxation time of 2.8 s.

The apparent hydrogen indexes (HI) that are reported in Table 1 were determined from the same CPMG transverse magnetization data for the three oils reported above, and also from relaxation data for an equal-volume sample of water. In each case, the amplitude of the first ten spin-echoes was extrapolated to evaluate the initial magnetization $M(0)$, and HI was calculated for the oil k as follows:

$$HI_k = M(0)_k / M(0)_{\text{water}}. \quad (47)$$

Linear and branched alkanes have higher H/C ratio than aromatic compounds. For this reason, the HI for Rice-1 and Rice-2 correlated well with their saturates:aromatics ratios (Table 1). The relatively low HI of Rice-3 is mostly influenced by the fast relaxation of heavy components such as asphaltenes. In this case, a fraction of the proton magnetization is lost before the first echo is acquired. For this reason, the apparent HI of heavy oils decreases with the API gravity [30].

Fig. 4 shows results from PGSE measurements for Rice-1, Rice-2 and water ($g = 0.131, 0.161$ and 0.025 T/m, respectively; $\Delta = 50$ ms and $\delta = 0-20$ ms in all cases), plotted in the usual way of logarithm of the attenuation ratio R vs. $\delta^2(\Delta - \delta/3)$ [16]. If Eq. (19) holds, such a plot should render a straight line. This is clearly the case for water, and nearly so for Rice-1. From the slope of the plot for water, a self-diffusion coefficient of 2.28×10^{-9} m²/s was determined. This value agrees well with $D = 2.3 \times 10^{-9}$ m²/s reported earlier for water at 25 °C.

The non-linear trend of the data for Rice-2 indicates that the oil exhibits a distribution of diffusion coefficients p_D . The lognormal p.d.f. has been used to correlate diffusion coefficients in crude oils [27], and we have adopted it to correlate

the PGSE data shown in Fig. 4:

$$p_D(D) = \frac{1}{D\sigma_D(2\pi)^{1/2}} \exp\left\{-\left[\frac{\ln(D) - \ln(D_{LM})}{2\sigma_D^2}\right]^2\right\} \quad (48)$$

where D_{LM} and σ_D are the logarithmic-mean diffusion coefficient and the geometric standard deviation of the distribution, respectively. Table 1 summarizes the values of D_{LM} and σ_D that rendered the best fit of the data for Rice-1 and Rice-2 (dashed lines in Fig. 4). D_{LM} is very close for both oils (1.78×10^{-10} and 1.75×10^{-10} m²/s, respectively), and an order of magnitude smaller than that of water. However, the width of the distribution is significantly larger for Rice-2. The short relaxation times of Rice-3 did not allow the characterization of this oil via PGSE. Instead, D_{LM} was estimated with the so-called constituent viscosity model [27], which correlates diffusivity, temperature and shear viscosity η as follows:

$$D_{LM} = \frac{bT}{\eta}. \quad (49)$$

In absence of experimental data, $b = 5.05 \times 10^{-15}$ Pa m² K⁻¹ was suggested for crude oils. This expression is an empirical modification of the well-known Stokes–Einstein equation. From Eq. (49) and the data reported in Table 1, $D_{LM} = 7.3 \times 10^{-12}$ m²/s is estimated for Rice-3.

7.2. Validation of Eq. (32)

Fig. 5 shows (symbols) PGSE measurements for samples of water and Rice-2 contacted as bulk fluids, not emulsified. The parameters used in the PGSE tests are also reported in Fig. 5. These parameters were chosen to assure only partial attenuation of the oil phase at the time the spin-echo was acquired. Three different compositions ($\phi_w = 0.25, 0.50$ and 0.75) were tested. The dashed lines stand for calculations of the decay of the attenuation ratio that would be expected for the pure water and the crude oil using Eqs. (19) and (34), respectively, and the diffusion coefficients reported above. No correction for restricted diffusion in the oil phase was made for these calculations. Data indicate that as the water content was increased, the attenuation ratio departed from that of the oil phase (R_O) and approached that of water phase (R_W), as might be expected.

The solid lines in Fig. 5 are predicted attenuation ratios for the mixture not emulsified, R_{MIX} , according to Eq. (32):

$$R_{MIX} = (1 - \kappa)R_W + \kappa R_O. \quad (50)$$

Eq. (50) is obtained from Eq. (32) by choosing arbitrarily the oil phase as the continuous phase. It can be shown that the calculation of R_{MIX} for bulk fluids in

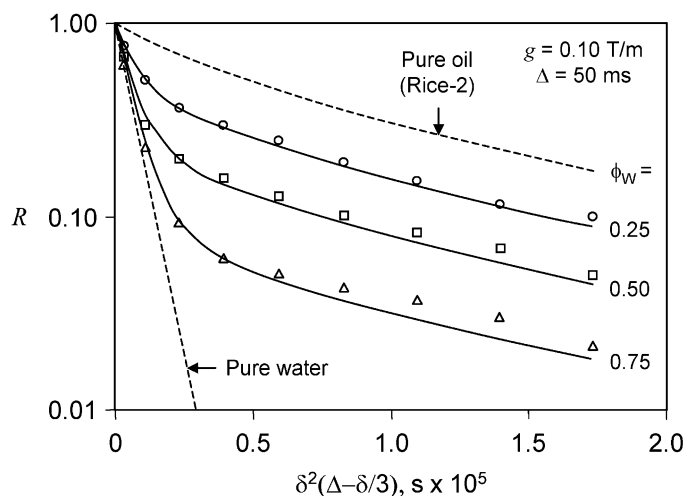


Fig. 5. PGSE results for mixtures of water and Rice-2 at several water-oil compositions. Experiments were performed at constant g and Δ , and varying δ ($\delta=0$ – 16 ms). No parameters have been adjusted in the calculations and the comparison with the experimental data is absolute.

contact in is independent of such choice. Clearly, this remark does not apply to emulsions.

The following values of $1-\kappa$ were calculated with Eq. (33) and the data for the pure fluids reported above: 0.522, 0.766 and 0.908 for $\phi_w=0.25$, 0.50 and 0.75, respectively. That is, 52.2%, 76.6% and 90.8% of R_{MIX} was given by the attenuation of the signal from the aqueous phase in each case, respectively. Good agreement was found between experiments and theory in all cases.

Fig. 6 shows results from three PGSE experiments on a mixture of Rice-2 and water ($\phi_w=0.50$). In this case, the strength of the magnetic field gradient g was modified. It was found that the trends for the attenuation ratio of the mixture exhibit a steeper decay as g increased. It was already mentioned that the pulsed magnetic field gradient imposes an inhomogeneous magnetic field on the sample during the time δ that causes loss of coherence in the ensemble of spins. For this reason, the amplitude of the spin-echo and, therefore, R diminish when g is augmented.

The dashed lines in Fig. 6 are calculations for the attenuation ratio of pure water using Eq. (19). The solid lines are the predicted profiles for the water/oil mixture, which were calculated as above (Eq. (50)). The parameter κ is independent of g ($\kappa=1-0.766=0.234$ in all cases). Therefore, differences between predicted profiles are determined by the effect of g on R_w and R_o . It is seen in Fig. 6 that the model correlated well the experimental data in all cases. Moreover, this figure also illustrates that a significant error would be made if the contribution of the magnetization of the oil phase to the attenuation ratio of the mixture is neglected, i.e. if R_{MIX} is said to depend only on R_w .

Fig. 7 shows (symbols) results from PGSE experiments on mixtures of water

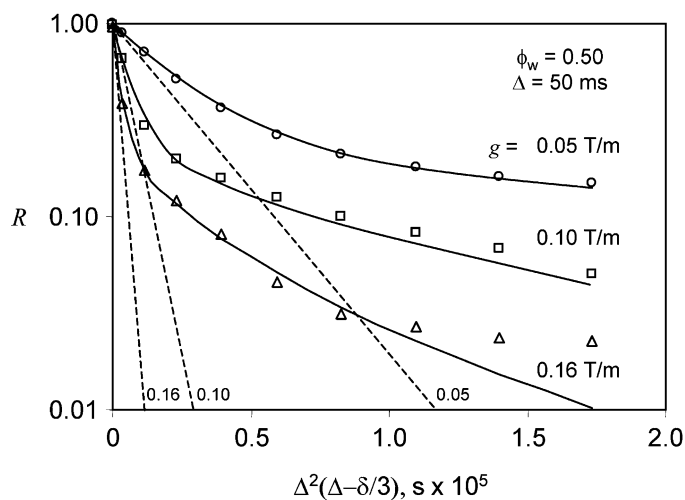


Fig. 6. PGSE results for a mixture of water (50 vol.%) and Rice-2 contacted as bulk fluids, not emulsified. Measurements were performed at different strengths of the magnetic field gradient and $\delta=0\text{--}16$ ms.

with each of the oils used in this study at fixed composition ($\phi_w=0.50$). The calculated attenuation profile for pure water is also plotted (dashed line). This figure suggests that the attenuation ratio was dominated by the signal from the water phase as the characteristic relaxation time of the oil decreased. Smaller signal was collected from the oil phase in the spin-echo when the oil exhibited faster relaxation (i.e. shorter $T_{2,LM}$).

The solid lines in Fig. 7 stand for the predicted profiles for each of the systems using Eq. (50). In support of the explanation given above, the calculated values of κ were 0.283, 0.234 and 0.014 for the Rice-1/water, Rice-2/water and Rice-3/water systems, respectively. The agreement between experiments and theory was satisfactory.

The experiments depicted in Fig. 5 through 7 demonstrate that the weighted average for R_{MIX} that is obtained from Eq. (50) correctly predicts the trend for the attenuation ratio of water/oil mixtures, independently of the composition of the mixture, of the type of oil that is used and of the PGSE parameters chosen for the test. The model is based on fundamental concepts of NMR spectroscopy and does not require adjustable parameters.

Fig. 8 shows (circles) experimental data for a sample containing water (10 vol.%) and Rice-1 (90 vol.%) in contact as bulk fluids, and for a w/o emulsion (squares) made from the same water/Rice-1 mixture. Test conditions were $g=0.131$ T/m, $\Delta=50$ ms and $\delta=0\text{--}16$ ms. The emulsion was ultrasonicated until the drop sizes were below the resolution limit of the PGSE experiment, which is $d_{MIN} \sim 3$ μm , according to Eq. (38). The mean drop size was followed via microphotography, and the final emulsion exhibited a narrow distribution of droplets with sizes close to the

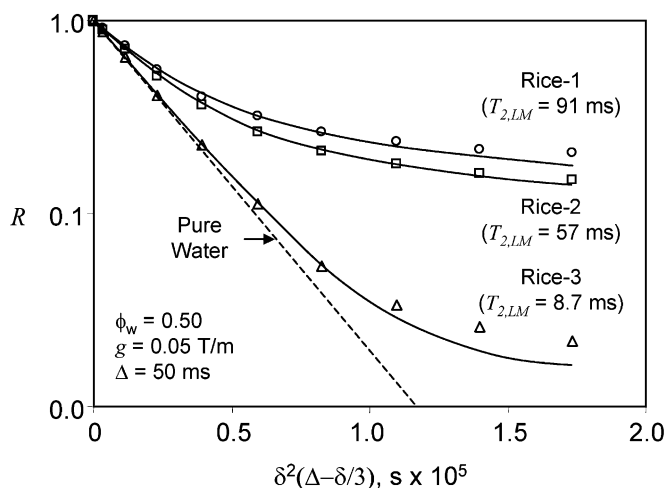


Fig. 7. PGSE results for mixtures of water (50 vol.%) and Rice-1, Rice-2 and Rice-3 contacted as bulk fluids, not emulsified ($\delta = 0\text{--}16$ ms).

resolution limit of the $40\times$ objective used in this study, i.e. $0.5\ \mu\text{m}$. The increase in the attenuation ratio that is observed for the emulsion with respect to the corresponding mixture of bulk fluids is caused by restricted diffusion of water molecules, which is imposed by the size of the droplets.

The dotted curve in Fig. 8 shows the predicted behavior for the sample before emulsification using Eq. (50). The attenuation ratio for either phase was calculated as indicated in the former experiments. In this case, $\kappa = 0.755$ was calculated from Eq. (33), which indicates that 75.5% of the attenuation ratio of the mixture is given by the oil phase.

The predicted behavior for the attenuation ratio of the emulsion via Eq. (32) is also shown (continuous line). Since water is the drop phase, $R_{\text{EMUL}} = (1 - \kappa)R_W + \kappa R_O$. The attenuation ratio R_W was not calculated from Eq. (19) (free diffusion), but from Eq. (23) because water molecules are confined in droplets with sizes below the resolution limit of the test. Therefore, if $d = 0.5\ \mu\text{m}$ as reported above, $R_W = 1 - 2 \times 10^{-4} \delta(s) \sim 1$. The attenuation ratio of the oil phase was calculated with Eqs. (34) and (48), using the parameters D_{LM} and σ_D given in Table 1 for Rice-1. Restricted diffusion in the oil phase was considered by correcting the logarithmic-mean diameter D_{LM} in Eq. (48) with the obstruction factor $\zeta = 0.952$ (Eq. (36)). Good agreement was found between experiments and calculations. These results show that Eq. (32) is valid for mixtures of bulk fluids and also for the emulsions.

The attenuation profile that would be obtained for the emulsion without considering the obstruction factor is also shown (dashed line). The effect of this correction is very small due to the relatively low drop phase content. In any case, these calculations correctly indicate that restricted diffusion in the continuous phase would increase the attenuation ratio of the emulsion.

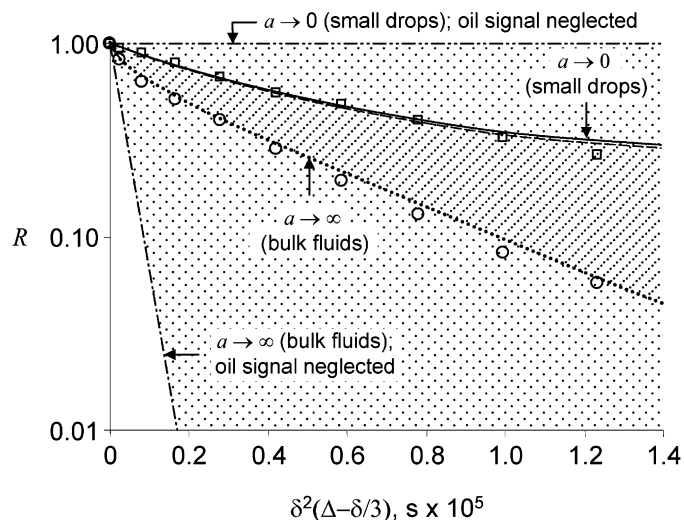


Fig. 8. Effect of the transverse magnetization of the continuous phase on the PGSE response of mixtures of water and Rice-1, contacted as bulk fluids and emulsified. The features of the plots are explained in the text.

The dash-dot and dash-dot-dot lines in Fig. 8 stand for the attenuation profiles that would be obtained for the same system before and after emulsification, respectively, if the contribution of the oil signal to the spin-echo amplitude is neglected. The area of the plot between these two lines has been shaded in light tone to indicate the range of conditions in which the attenuation ratios for emulsions with any given drop size distribution could be found if the oil signal were indeed negligible, i.e. if Eq. (26) were correct. If Eq. (32) holds instead as experiments suggest, such conditions are restricted to the area shaded in dark tone. Clearly, neglecting the signal from the oil phase would lead to significant error in the prediction of the attenuation profile for this system. The trends shown in Fig. 8 have been confirmed in experiments with other water/oil mixtures.

It is worth noting that the parameters of a PGSE experiment should be chosen in order to *minimize* the effect of the continuous phase on the spin-echo and, therefore, on the attenuation ratio of the emulsion, while maintaining a satisfactory signal-to-noise ratio. The idea is to broaden the range of conditions at which attenuation ratios can be obtained (this is, to expand the extension of the dark-shaded area in Fig. 8), so the uncertainty in the drop size distribution that is determined from the PGSE diminishes. Therefore, Eq. (32) can be used as a tool to predict limiting attenuation profiles and optimize the selection of parameters for PGSE tests.

7.3. The combined CPMG–PGSE method in practice

Fig. 9a shows the T_2 distribution of a sample of Rice-2 (dotted line) and also of a mixture of water (30 vol.%) and Rice-2 in contact, not emulsified (solid line). It

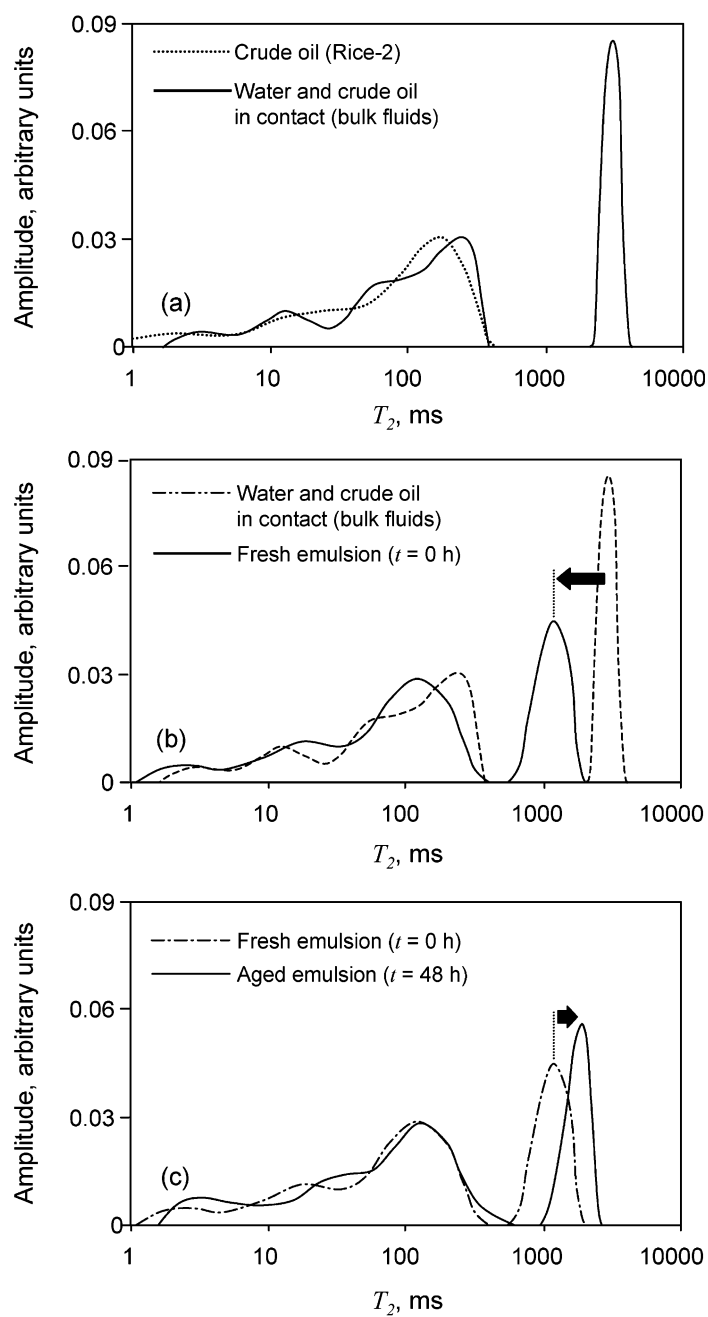


Fig. 9. T_2 distribution of mixtures of water (30 vol.%) and Rice-2, contacted as bulk fluids and emulsified.

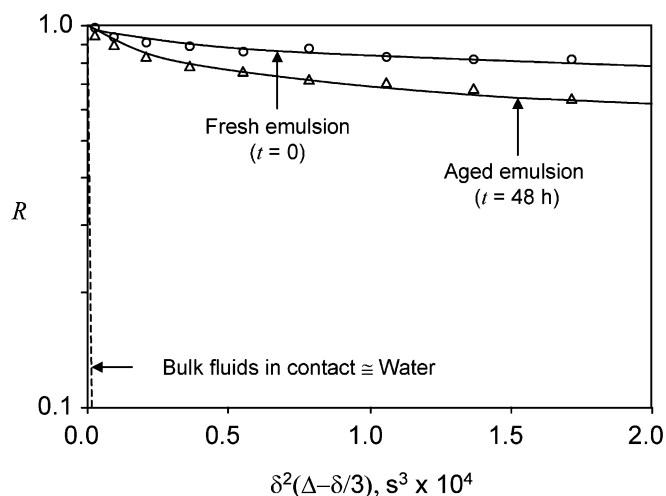


Fig. 10. PGSE data for fresh ($t=0$) and aged ($t=48$ h) emulsions of water (30 vol.%) in Rice-2.

is seen that the position of the oil peak is not affected by the presence of water. The water signal is shown as a narrow peak with logarithmic mean of 3.0 s.

Fig. 9b shows the same T_2 distribution of the water/oil mixture (dashed line) mentioned above, and also of the same sample right after dispersing the system to form a w/o emulsion (solid line). The most relevant feature of Fig. 9b is that emulsification leads to a significant displacement of the water signal toward shorter relaxation times. This difference in relaxation times can be explained by an enhanced decay of transverse magnetization at the water–oil interfaces (surface relaxation), in connection with the increase of interfacial area that results from the formation of droplets.

Fig. 9c shows the T_2 distribution of the same emulsion 48 h after emulsification (solid line). The T_2 distribution for the fresh emulsion (dash-dot line) is also included for comparison. In this case, the relaxation times of the water phase increase because, as drop sizes grow and phase separation takes place, the interfacial area diminishes and the contribution of surface relaxation to the decay of magnetization is reduced.

In the CPMG experiments that originated the results depicted in Fig. 9, 16 stacks were accumulated and an average noise level of 0.45% was obtained. It took 4.7 min to complete each test.

Fig. 10 shows results from PGSE experiments on the emulsions discussed above at $t=0$ (circles) and $t=48$ h (squares). The parameters used for these tests were $g=0.10$ T/m, $\Delta=0.2$ s, $\delta=0-0.04$ s. The profile that would be obtained for the mixture before emulsification (R_{MIX}) was calculated using Eq. (50) and is also plotted in Fig. 10 (dashed line). In this case, $\kappa=0.0025$, i.e. the oil phase had relaxed almost completely at $t=2\tau$, and the attenuation ratio of the mixture was nearly that of the water phase ($R_{\text{MIX}} \sim R_w$). Emulsification led to a significant

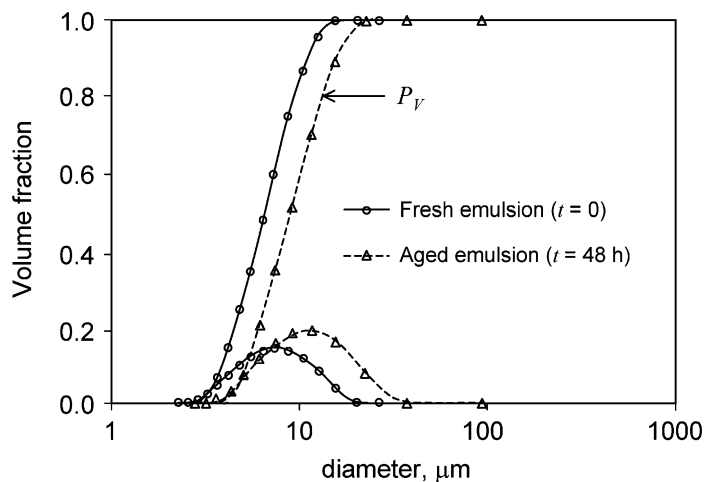


Fig. 11. NMR results for the drop size distribution of fresh ($t=0$) and aged ($t=48$ h) emulsions of water (30 vol.%) in Rice-2.

increase in the attenuation ratio of the emulsion, when compared to R_{MIX} , due to restricted diffusion of water molecules within the drops. The reduction in the attenuation ratio from fresh to aged emulsion indicates an enlargement of the average displacement in the spins, and suggests an increase in droplet sizes.

The drop size distributions shown in Fig. 11 were calculated from the CPMG and PGSE data given in Figs. 9 and 10, respectively, and following the combined procedure explained above. The solid lines in Fig. 10 stand for the calculated profile for the attenuation ratios that are obtained with Eq. (32) and these distributions of sizes. It is seen in Fig. 11 that the volume-weighted mean size of the emulsion increased from 6.9 to 8.8 μm . Also, the width of the distribution remained practically unchanged. This example illustrates that both CPMG and PGSE are suitable to study the stability of emulsions.

Once the drop size distribution is determined, it is important to verify that the fast diffusion approximation is valid. The following surface relaxivities (ρ) were determined from the combined CPMG-PGSE procedure for these emulsions: 0.66 $\mu\text{m/s}$ ($t=0$) and 0.48 $\mu\text{m/s}$ ($t=48$ h). In addition, the largest drop diameters that were measured were 22 μm ($t=0$) and 45 μm ($t=48$ h), as shown in Fig. 11. Therefore,

$$\left. \frac{\rho a_i}{D} \right|_{t=0} \leq 0.007; \quad \left. \frac{\rho a_i}{D} \right|_{t=48 \text{ h}} \leq 0.010.$$

These figures are well below the practical limit for fast diffusion established in Eq. (6). For this reason, it can be said that the effect of surface relaxation on the changes in the attenuation profiles shown in Fig. 10 was negligible.

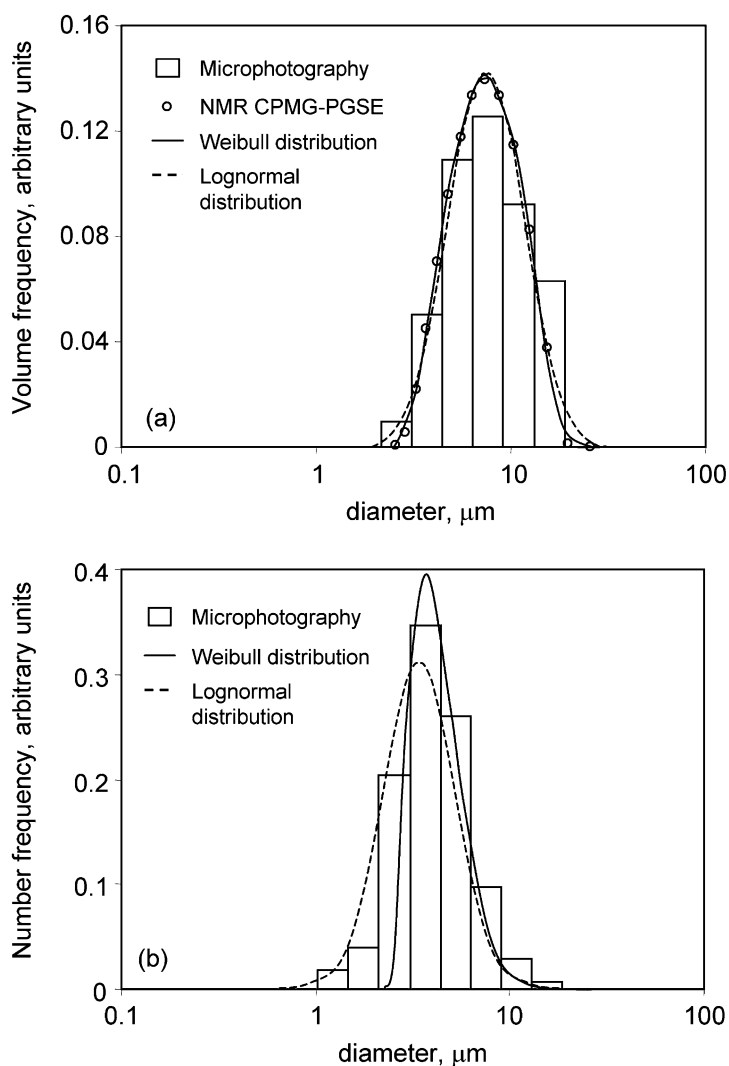


Fig. 12. Drop size distribution of the fresh emulsion: comparison of NMR and microphotography results.

Fig. 12a compares the results from the NMR technique (circles) with measurements on the drops size distribution via microphotography (bars) for the fresh emulsion. Results are reported based on the volume of droplets. The volume-weighted mean size of the distribution determined via microphotography was 7.7 μm . This result is in good agreement with the NMR results (6.9 μm , see above). The agreement is also satisfactory for the width of the distribution. The solid and dashed lines in Fig. 12a stand for the best fit to the CPMG data of the bimodal Weibull (Eqs. (40) and (41)) and lognormal (Eqs. (25) and (42)) distributions,

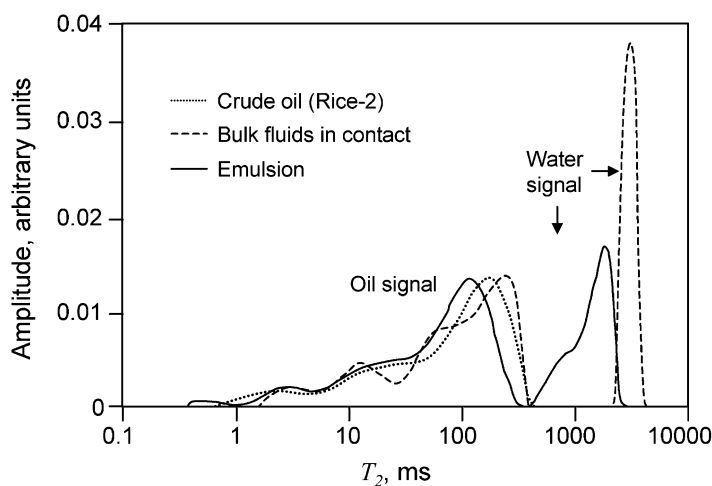


Fig. 13. T_2 distribution of a blend of two emulsions of water (30 vol.%) in Rice-2.

respectively. With the parameters that are determined from the fitting procedure (lognormal: $d_{gV} = 6.9 \mu\text{m}$; $\sigma = 0.424$; Weibull: $\omega = 0.8228$; $m_1 = 2.9381$; $m_2 = 6.2584$; $\sigma_1 = 1.0775$; $\sigma_2 = 1.5504$; $a_0 = 1.21 \mu\text{m}$), the number-based drop size distribution $p_N(a)$ can be calculated according to:

$$p_N(a) = a^{-3} p_V(a) / \int_0^{\infty} a^{-3} p_V(a) da \quad (51)$$

Fig. 12b compares the number-based drop size distribution via microphotography (bars) with those calculated from the bimodal Weibull (solid line) and lognormal (dashed line) fits of the CPMG data. The medians of these distributions are 4.2, 4.5 and 4.0 μm , respectively. Good agreement is observed in both cases, although it is noted that the lognormal function exhibited better correlation of small sizes in this experiment.

The ability of the PGSE-CPMG method to account for drop size distributions not exhibiting a lognormal shape was tested by mixing equal volumes of two emulsions of water in Rice-2, both containing 30 vol.% water. Each emulsion was made following a different emulsification procedure. The first emulsion was stirred and the second was stirred and further ultrasonicated according to the protocol described above.

Fig. 13 shows the T_2 distribution of the mixed emulsion (solid line). Two independent peaks were obtained, one corresponding to the oil signal between 0.4 and 316 ms, and another to the water phase between 383 and 2610 ms. The T_2 distributions of a sample of Rice-2 (dotted line), and of a mixture of water (30 vol.%) and Rice-2 contacted as bulk fluids (dashed line) are also included. Again, the shift in the water peak toward low relaxation times is caused by surface

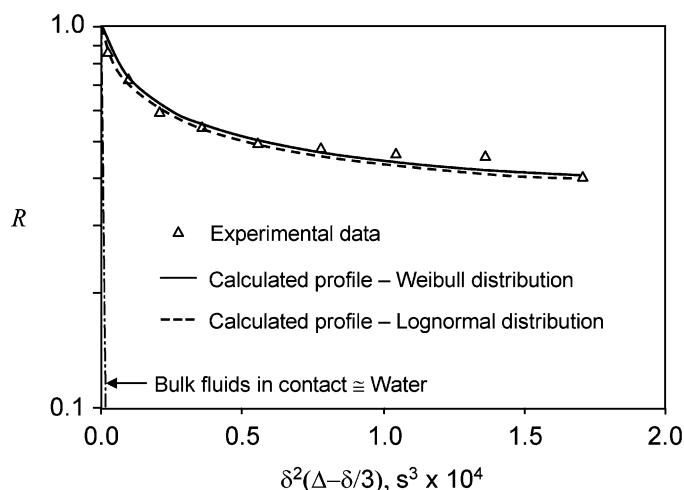


Fig. 14. PGSE data for the blend of two emulsions of water (30 vol.%) in Rice-2.

relaxation. In these experiments, 16 stacks were accumulated and an average noise level of 0.30% was obtained. It took 4.7 min to complete each test.

Fig. 14 exhibits (triangles) the experimental decay of the attenuation ratio R that were obtained from the PGSE experiment on the mixed emulsion. The same parameters of the previous test were chosen. Also, $\kappa=0.0025$ as before. The solid line corresponds to the best fit of the PGSE data that was obtained using Eq. (32) and the Weibull fit of the drop size distribution that was calculated from the T_2 distribution. The dashed line corresponds to the same fit, but using the lognormal p.d.f. for the correlation of the drop size distribution instead.

Fig. 15a reports results for the volume-weighted drop size distribution, measured via microphotography (bars) and NMR-CPMG (circles) with $\rho=0.88 \mu\text{m/s}$. The solid line stands for the best fit to the CPMG drop size distribution data using the bimodal Weibull p.d.f., and the dashed line is the best fit to the same data with the lognormal p.d.f. The following parameters were obtained in each case: lognormal, $d_{gV}=13.0 \mu\text{m}$; $\sigma=0.756$; Weibull, $\omega=0.3838$; $m_1=2.0288$; $m_2=4.9783$; $\sigma_1=1.2047$; $\sigma_2=2.2063$; $a_0=1.15 \mu\text{m}$. With these parameters, the number-based drop size distribution was calculated and plotted together with the microphotography data in Fig. 15b. From this figure it becomes clear that the usage of the lognormal p.d.f. can lead to errors in the characterization of the drop size distribution for systems in which lognormality is not observed. The proposed form of the Weibull distribution gave a satisfactory estimation of $p_N(a)$.

It is worth noting that the shapes of the Weibull and lognormal plots in Fig. 15 were significantly different, yet the predicted attenuation decays that are calculated from such plots and reported in Fig. 14 were very similar. This feature indicates that it is not always adequate to resolve for the shape of the drop size distribution from a reduced PGSE dataset. In general, The T_2 distribution that is obtained from

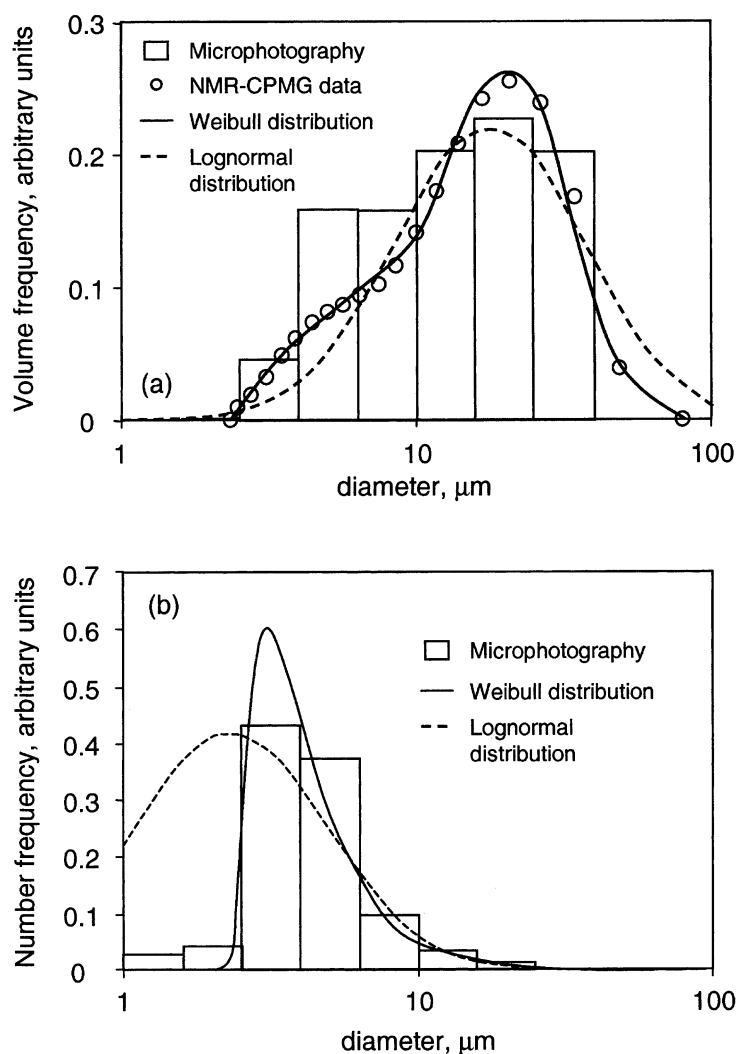


Fig. 15. Drop size distribution of the blend of two emulsions of water (30 vol.%) in Rice-2: comparison between NMR and microphotography results.

a CPMG test is more sensitive than the attenuation profile measured from a corresponding PGSE experiment to the shape of the drop size distribution. For this reason, we recommend estimating the shape of the drop size distribution from CPMG data, and not from PGSE measurements as reported by Ambrosone et al. [54,55].

Figs. 16–18 summarize an example of the application of the combined method to a bimodal emulsion of water (30 vol.%) in Rice-3. In this case, the emulsion

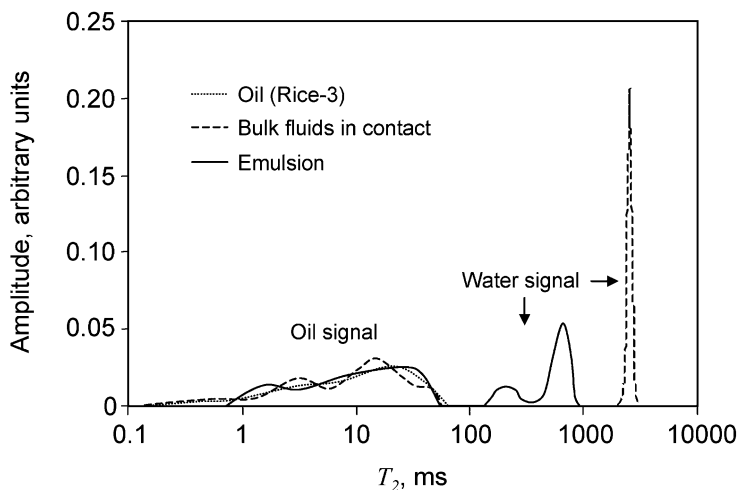


Fig. 16. T_2 distribution of a bimodal emulsion of water (30 vol.%) in Rice-3.

was made with mechanical stirring, and ultrasonication was applied at a particular location of the emulsion to cause a local reduction in drop sizes. The procedure was repeated until a second peak in the water signal of the T_2 distribution appeared (Fig. 16). In these experiments, 16 stacks were accumulated and an average noise level of 0.42% was obtained. It took 4.7 min to complete each test. A bimodal distribution of drop sizes was obtained (Fig. 18), in correspondence with the bimodal T_2 distribution of the drop phase. The parameters of the PGSE test were

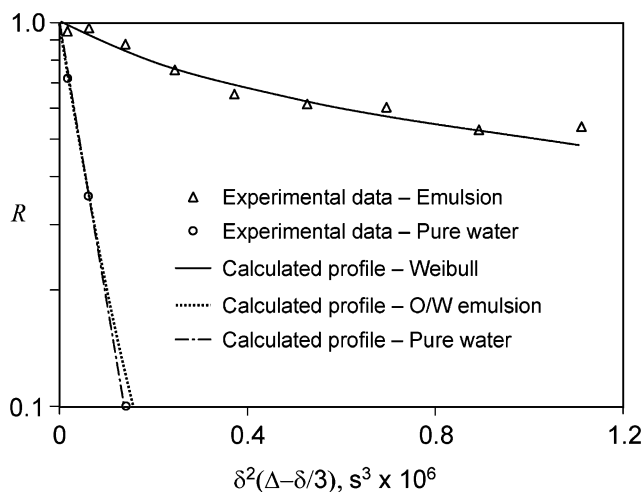


Fig. 17. PGSE data of a bimodal emulsion of water (30 vol.%) in Rice-3.

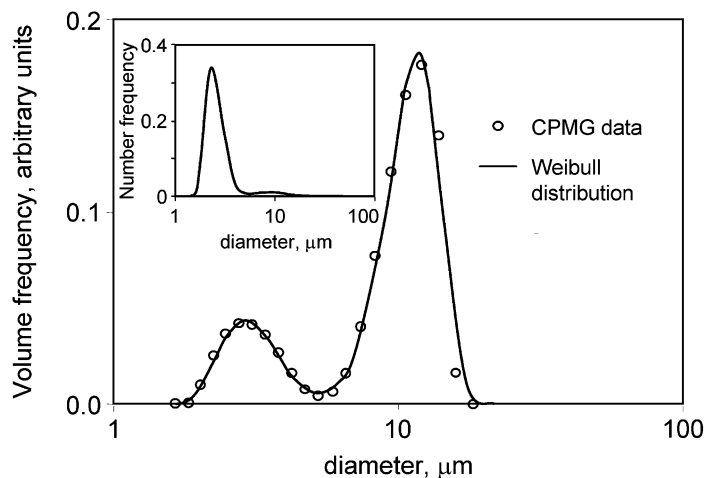


Fig. 18. Volume-weighted and number-based drop size distribution of a bimodal emulsion of water (30 vol.%) in Rice-3.

$g=0.327$ T/m, $\Delta=0.02$ s, $\delta=0-0.008$ s. In addition, $\kappa=0.0259$ according to Eq. (33). The fit of the CPMG drop size distribution with the Weibull p.d.f. rendered the following parameters: $\omega=0.7612$; $m_1=9.9399$; $m_2=2.6876$; $\sigma_1=1.9042$; $\sigma_2=0.6057$; $a_0=0.832$ μm . A lognormal fit of the CPMG data is inadequate in this case, since it would render a unimodal distribution. The surface relaxivity measured in this experiment was 2.18 $\mu\text{m/s}$.

7.4. Morphology of the emulsion

NMR allows screening if an emulsion is *w/o* or *o/w* in a straightforward manner. The experimental data shown in Fig. 17 (triangles) were fitted (solid line) assuming that the emulsion is water-in-oil. If the opposite (*o/w*) configuration were considered instead, the profile shown as a dotted line would be obtained. In the latter case, the response of the *o/w* emulsion would be very close to that of bulk water, because water is now the continuous phase and the contribution of the oil phase to the attenuation ratio is very small as discussed above. Therefore, the notorious difference between attenuation profiles can be used to infer the morphology of the emulsion.

The basis for the discrimination of the emulsion type via attenuation ratio profiles is the contrast in self-diffusivities between the oil and water phases. For systems in which D_w and D_o are similar, the resolution of the morphology of the emulsion with this method is not clear-cut.

7.5. Oil/water composition

Thirty *w/o* emulsions were prepared using each of the crude oils at increasing water/oil ratios, and a CPMG experiment was performed on each sample. Fig. 19

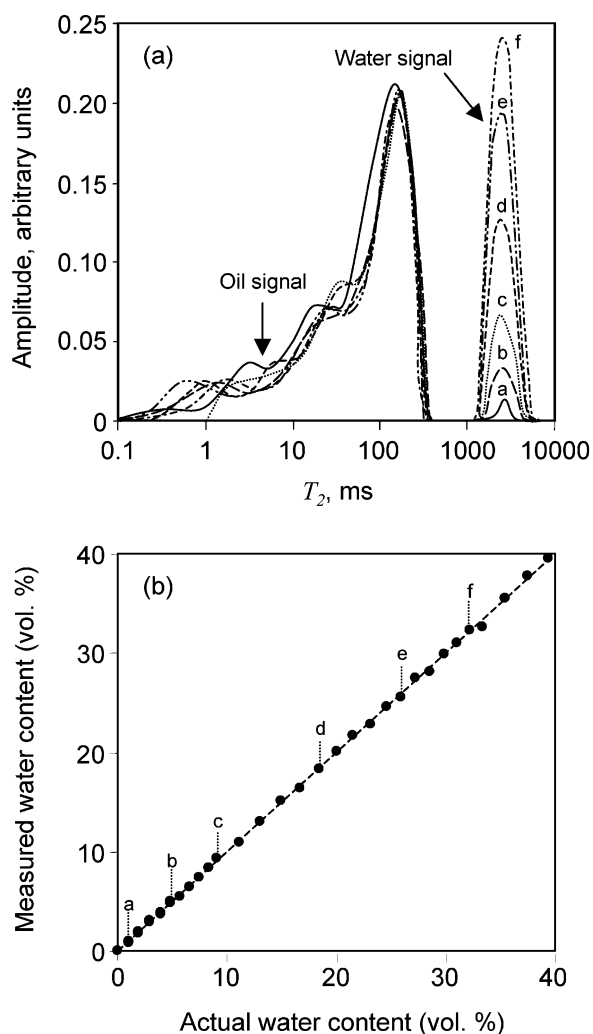


Fig. 19. Determination of water composition via CPMG. (a) T_2 distribution of selected emulsions of water in Rice-2. Data were normalized with respect to the oil signal; (b) comparison between actual and NMR-measured water contents.

shows results for water/Rice-2 emulsions. Fig. 19a illustrates the T_2 distribution of six of these samples. The actual water content was in each case (a) 1.0 vol.%; (b) 4.8 vol.%; (c) 9.1 vol.%; (d) 18.4 vol.%; (e) 26.0 vol.%; (f) 32.2 vol.%. Data are shown normalized with respect to the oil signal. In these experiments, the water/oil mixtures were gently shaken by hand to minimize formation of very small drops and prevent significant displacement of the T_2 signal of the water phase. This figure clearly illustrates how the signal from the water phase increases with the water

Table 2
Summary of surface relaxivities measured in this study

Oil phase	ρ ($\mu\text{m/s}$)	d_{gV} (μm)	σ	A + R (wt.%)	Fe (ppm)
Rice-1	0.39	20.0	0.60	10.50	2.4
	0.39	22.1	0.61		
	0.54	13.4	0.05		
	$\bar{\rho} = 0.46 \pm 0.08$				
Rice-2	0.48	8.8	0.42	16.62	7.9
	0.66	6.9	0.40		
	0.88	13.0	0.76		
	$\bar{\rho} = 0.68 \pm 0.20$				
Rice-3	2.17	8.6	0.47	48.7	51
	2.01	8.1	0.55		
	2.06	9.1	0.33		
	$\bar{\rho} = 2.09 \pm 0.08$				

A + R = Content of asphaltenes and resins in topped oil (wt.%), as reported in Table 1.

d_{gV} , σ = Volume-weighted mean size and geometric standard deviation of the drop size distribution from which ρ is calculated (best fit with lognormal distribution).

content, as might be expected. Fig. 19b compares the actual water content of these and other mixtures with the water content that is calculated with Eq. (17). The calculated ϕ_w for the systems considered in Fig. 19a were: (a) 0.9 vol.%; (b) 4.8 vol.%; (c) 9.3 vol.%; (d) 18.4 vol.%; (e) 25.7 vol.%; (f) 32.4 vol.%. Excellent agreement was found between actual and measured water contents, with errors averaging ± 0.2 vol.%.

Finally, calculations were performed with synthetic data to assess the accuracy of this method. Noise levels of 0, 0.1, 1.0, 3.0 and 5.0% were tested, and ten simulated experiments were run on a hypothetical emulsion of water (35 vol.%) in Rice-3 for each noise level. The maximum error in the water content calculated from the synthetic relaxation data was 0%, 0.2%, 1.0%, 1.5% and 4.0%, respectively. These simulations suggest that the uncertainty of the water content corresponds roughly to the noise level.

7.6. Surface relaxivities

Table 2 summarizes surface relaxivity measurements on emulsions of water in Rice-1, Rice-2 and Rice-3, along with selected composition data from Table 1. Data suggests that asphaltenes, resins and paramagnetic materials may play a role in the prevailing relaxation mechanism, since ρ increased monotonically with the content of asphaltenes and resins (A + R), and also Fe in the crude oil. Asphaltene-resin structures exhibit surface activity and might be expected to adsorb at the water-oil interfaces. Protons of these structures appear to exhibit short relaxation time constants [29] and they may well contribute to increase surface relaxivity in the water-in-crude oil emulsion. Paramagnetic ions adsorbed at the interfaces in the water-in-crude oil emulsion would also increase ρ . However, no conclusive relationships

between mean drop size, polydispersity and surface relaxivity was observed for the few systems reported in Table 2.

The surface relaxivities of these emulsions are low with respect to those found for sandstones (approx. 5–20 $\mu\text{m/s}$) [31], but are still comparable to those of SiO_2 and SiC grain packs and other natural rocks [83]. This result may have implications to NMR characterization of multiphase flow in porous media because the assumption that is often made of negligible surface relaxivity at the liquid–liquid interfaces with respect to that at the rock–fluid interfaces may not be adequate in all practical cases.

It is worth noting that the calculations of the attenuation ratios for the drop phase in the PGSE experiments were made using Eq. (20), i.e. neglecting the effect of surface relaxation on R . The calculations were also performed taking into account this effect with Eq. (30). In all cases, the difference between R_{sp} and $R_{\text{sp},\rho}$ was equal to or less than 0.002. This figure illustrates that it is appropriate to neglect the effect of ρ on the attenuation ratio when PGSE measurements are performed in the fast diffusion mode.

Callaghan [84] has developed a matrix formalism to interpret restricted diffusion data from pulsed sequences with gradient pulses of arbitrary shape, of which the finite-width gradient pulse PGSE is a particular case. Codd and Callaghan [85] have extended such formalism to account for surface relaxation at the walls of spheres. These authors noted that when $\rho=1\text{--}10$ $\mu\text{m/s}$ and the magnetization data is collected from water confined in pores of the order of 10 μm , the effect of surface relaxation on the attenuation ratio can be neglected. The small difference between calculations from Eqs. (20) and (30) that was reported above concurs with this assessment.

Finally, it is worth mentioning that the combined method is useful whenever the contribution of surface relaxation to the decay of transverse magnetization in CPMG tests is significant, as was shown for oilfield emulsions. We have performed preliminary tests on emulsions of water in lubricant oil free of paramagnetic impurities, and stabilized with non-ionic surfactants (SPAN 80, 5 wt.%). For such systems, surface relaxivities in the order of 0.2 $\mu\text{m/s}$ were measured. Not surprisingly, this figure is smaller than the surface relaxivities reported in Table 2. In any case, the applicability of the method for emulsions that may potentially exhibit low surface relaxivities, such as food emulsions, has not been fully ascertained.

8. Conclusions

A novel approach to process experimental data from classic NMR experiments for the characterization of water-in-oil emulsions has been proposed and tested in emulsions of water in crude oils. The method combines results from the PGSE and CPMG tests to render the drop size distribution of the emulsion, the water/oil ratio and the average surface relaxivity. To our knowledge, this is the first experimental procedure that is proposed in the general literature to determine the surface relaxivity at liquid–liquid interfaces. Obviously, ρ can be determined by combining CPMG

data with any independent measurement of the drop size distribution, not necessarily PGSE, but there is an evident benefit in performing such measurement with the same instrument and practically at the same time at which the CPMG test is done.

As part of the development of such method, the theoretical framework to calculate drop size distributions from CPMG data has been reviewed and expanded, and the classic theory for PGSE has been extended to take into account the general case in which the amplitude of the spin-echo is influenced by the transverse magnetization of the continuous and drop phases.

Acknowledgments

This research was supported by the J.W. Fulbright program (scholarship to A. P.), by OndeoNalco Energy Services, and by the Rice University Consortium for Processes in Porous Media. The authors also would like to thank Mr Mark Flaum, Dr John Shafer, Dr Keh-Jim Dunn and Dr Clarence Miller for useful suggestions and discussions.

Appendix A:

A.1. The ‘fast-diffusion’ limit in practice

Brownstein and Tarr [19] showed that the relaxation of the proton magnetization $M(t)$ of a pure, isotropic fluid confined in a sphere of radius a is given by the sum of decreasing exponential functions with positive intensity I_n :

$$M(t) = M(0) \sum_{n=0}^{\infty} I_n e^{-t/T_n}. \quad (52)$$

where

$$I_n = \frac{12(\sin\lambda_n - \lambda_n \cos\lambda_n)^2}{\lambda_n^3 [2\lambda_n - \sin(2\lambda_n)]}; \quad \sum_{n=0}^{\infty} I_n = 1, \quad (53)$$

$$\frac{1}{T_n} = \frac{1}{T_{\text{bulk}}} + \frac{\lambda_n^2 D}{a^2}, \quad (54)$$

and the eigenvalues λ_n are determined from:

$$\lambda \cot \lambda = 1 - \rho a / D. \quad (55)$$

Fig. 20 shows a plot of the first three intensities I_0 , I_1 and I_2 as a function of $\rho a / D$. In the limit of ‘fast-diffusion’ [$\rho a / D \ll 1$, see Eq. (5)], the first mode ($n=0$) dominates ($I_0 \rightarrow 1$; $\{I_1, I_2, \dots, I_n\} \rightarrow 0$) and the transient magnetization can be modeled using one exponential:

$$M_{\text{FDL}}(t) = M(0) e^{-t/T_0}. \quad (56)$$

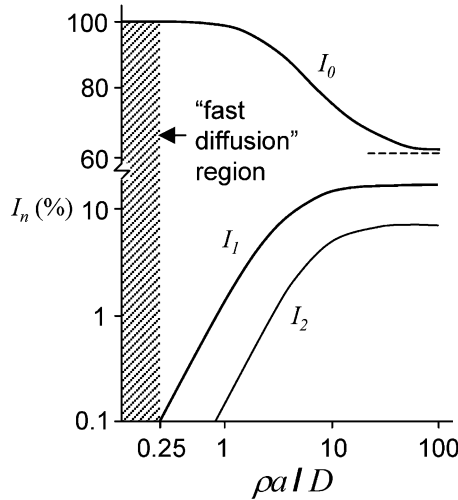


Fig. 20. Plot of the first three intensities I_0 , I_1 and I_2 of the magnetization of an isotropic fluid confined in a sphere. In the ‘fast diffusion’ mode, the first intensity I_0 dominates. Adapted from Ref. [19].

Also, it can be shown from Eq. (55) that when $\rho a/D \ll 1$, the first eigenvalue is given by:

$$\lambda_{0,\text{FDL}}^2 = 3\rho a/D - \frac{3}{5}(\rho a/D)^2 + O[(\rho a/D)^3]. \tag{57}$$

Eqs. (3) and (4) are obtained by replacing the first term in the right hand side of Eq. (57) in Eq. (54). The sub-index ‘2’ is added to denote transverse relaxation times:

$$\frac{1}{(T_0)_{\text{FDL}}} \equiv \frac{1}{T_2} = \frac{1}{T_{2,\text{bulk}}} + \rho \frac{3}{a} \quad \text{whence } a = 3\rho \left(\frac{1}{T_2} - \frac{1}{T_{2,\text{bulk}}} \right)^{-1}$$

when $\rho a/D = 0.24582\dots \sim \frac{1}{4}$ the intensity I_0 accounts for 99.9% of the initial magnetization (Fig. 20). We adopt this value for $\rho a/D$ as the threshold for the fast-diffusion regime.

Finally, it can be shown that the error that is made in the determination of drop sizes by neglecting the second and higher order term of Eq. (57) is $e(\%) \cong 20(\rho a/D)$. Therefore, Eq. (4) is exact for $\rho a/D \rightarrow 0$, and it overestimates the drop size by 5% when $\rho a/D = \frac{1}{4}$.

A.2. Derivation of Eq. 32 and particular cases

The amplitudes of the spin-echoes that are acquired in a PGSE experiment on emulsions in presence ($g > 0$) or absence ($g = 0$) of magnetic field gradient pulses are, respectively:

$$M_{\text{EMUL}}(2\tau, g > 0) = M_{\text{DP}}(2\tau, g > 0) + M_{\text{CP}}(2\tau, g > 0), \quad (58)$$

and

$$M_{\text{EMUL}}(2\tau, g = 0) = M_{\text{DP}}(2\tau, g = 0) + M_{\text{CP}}(2\tau, g = 0) \quad (59)$$

whence:

$$R_{\text{EMUL}} = \frac{M_{\text{DP}}(2\tau, g > 0) + M_{\text{CP}}(2\tau, g > 0)}{M_{\text{DP}}(2\tau, g = 0) + M_{\text{CP}}(2\tau, g = 0)}. \quad (60)$$

It is straightforward to show from Eq. (60) that:

$$R_{\text{EMUL}} = (1 - \kappa)R_{\text{DP}} + \kappa R_{\text{CP}}. \quad (61)$$

where R_{DP} and R_{CP} are the time-resolved attenuation ratios of the drop and continuous phases, respectively:

$$R_{\text{DP}} = \frac{M_{\text{DP}}(2\tau, g > 0)}{M_{\text{DP}}(2\tau, g = 0)}; \quad R_{\text{CP}} = \frac{M_{\text{CP}}(2\tau, g > 0)}{M_{\text{CP}}(2\tau, g = 0)} \quad (62)$$

The parameter κ ($0 \leq \kappa \leq 1$),

$$\kappa = \left[1 + \frac{M_{\text{DP}}(2\tau, g = 0)}{M_{\text{CP}}(2\tau, g = 0)} \right]^{-1}, \quad (63)$$

weights the relative contribution of R_{DP} and R_{CP} to the overall attenuation ratio of the emulsion.

Once the distribution of relaxation times of each phase are resolved from the T_2 distribution of the emulsion, κ can be calculated as follows,

$$\kappa = \left[1 + \frac{\sum (f_i)_{\text{DP}} \exp[-2\tau/(T_{2,i})_{\text{DP}}]}{\sum (f_i)_{\text{CP}} \exp[-2\tau/(T_{2,i})_{\text{CP}}]} \right]^{-1}, \quad (64)$$

After substituting Eqs. (3) and (16) in Eq. (64), we obtain:

$$\kappa = \left[1 + \frac{\phi_{\text{DP}} \text{HI}_{\text{DP}}}{\phi_{\text{CP}} \text{HI}_{\text{CP}}} \frac{\exp[-2\tau/(T_{2,\text{bulk}})_{\text{DP}}]}{\sum (x_i)_{\text{CP}} \exp[-2\tau/(T_{2,i})_{\text{CP}}]} \sum (x_i)_{\text{DP}} \exp[-6\tau\rho/a_i] \right]^{-1};$$

$$(x_i)_k = \frac{(f_i)_k}{\sum_j (f_j)_k}. \quad (65)$$

Eq. (65) can be simplified and κ computed from transverse relaxation data determined independently for each phase if the effect surface relaxation on the PGSE spin-echo is negligible. This is:

$$\kappa = \left[1 + \frac{\phi_{\text{DP}} \text{HI}_{\text{DP}}}{\phi_{\text{CP}} \text{HI}_{\text{CP}}} \frac{\exp[-2\tau/(T_{2,\text{bulk}})_{\text{DP}}]}{\sum (x_i)_{\text{CP}}^* \exp[-2\tau/(T_{2,i})_{\text{CP}}^*]} \right]^{-1} \quad (66)$$

Eq. (66) is valid if $a_m > \sim 2\tau\rho$, where a_m is the minimum drop size that can be determined from the T_2 distribution of the emulsion for which $f_i > 0$. In a typical PGSE experiment on emulsions, $2\tau = 100$ ms, $\rho = 0.5$ $\mu\text{m/s}$ and, therefore, $a_m > 0.05$ μm . For this reason, Eq. (66) provides a satisfactory value of κ in most practical cases. Furthermore, the natural relaxation of the continuous phase can be computed approximately in terms of its logarithmic-mean T_2 , $(T_{2,\text{bulk}})_{\text{CP}}$. If so, Eq. (66) becomes:

$$\kappa \cong \left[1 + \frac{\phi_{\text{DP}} \text{HI}_{\text{DP}}}{\phi_{\text{CP}} \text{HI}_{\text{CP}}} \frac{\exp[-2\tau/(T_{2,\text{bulk}})_{\text{DP}}]}{\exp[-2\tau/(T_{2,\text{bulk}})_{\text{CP}}]} \right]^{-1} \quad (67)$$

Eq. (67) is useful to illustrate the two limiting cases for κ . Firstly, $\kappa \rightarrow 0$ for highly concentrated emulsions ($\phi_{\text{CP}} \rightarrow 0$), or for mixtures in which the continuous phase has relaxed completely at the time the spin-echo is acquired, because $\exp[-2\tau/(T_{2,\text{bulk}})_{\text{CP}}] \rightarrow 0$. In this case, Eq. (32) correctly reduces to Eq. (26), i.e. R_{EMUL} is determined only by the attenuation ratio of the drop phase. Conversely, $\kappa \rightarrow 1$ (and $R_{\text{EMUL}} = R_{\text{CP}}$ according to Eq. (32)) for very dilute emulsions ($\phi_{\text{DP}} \rightarrow 0$), or for mixtures in which the drop phase has relaxed completely at the time the spin-echo is acquired since $\exp[-2\tau/(T_{2,\text{bulk}})_{\text{DP}}] \rightarrow 0$.

References

- [1] P. Walstra, Emulsion stability, in: P. Becher (Ed.), Encyclopedia of Emulsion Technology, Vol. 4, Marcel Dekker, New York, 1996, chapter 1.
- [2] A.A. Peña, C.A. Miller, Transient behavior of polydisperse emulsions undergoing mass transfer, Ind. Eng. Chem. Res. 41 (2002) 6284–6296.

- [3] Y. Otsubo, R.K. Prud'homme, Effect of drop size distribution on the flow behavior of oil-in-water emulsions, *Rheol. Acta* 33 (1994) 303–306.
- [4] M. Ramírez, J. Bullón, J. Andérez, I. Mira, J.L. Salager, Drop size distribution and its effect on O/W emulsion viscosity, *J. Disp. Sci. Technol.* 23 (2002) 309–321.
- [5] R. Pal, Effect of droplet size on the rheology of emulsions, *AIChE J.* 42 (1996) 3181–3190.
- [6] D.J. McClements, Theoretical prediction of emulsion color, *Adv. Colloid Interface Sci.* 97 (2002) 63–89.
- [7] D. Kilcast, S. Clegg, Sensory perception of creaminess and its relationship with food structure, *Food Qual. Pref.* 13 (2002) 609–623.
- [8] S.M. van Ruth, G. de Vries, M. Geary, P. Giannouli, Influence of composition and structure of oil-in-water emulsions on retention of aroma compounds, *J. Sci. Food Agric.* 82 (2002) 1028–1035.
- [9] M. Charles, V. Rosselin, L. Beck, F. Sauvageot, D. Guichard, Flavor release from salad dressings: sensory and physicochemical approaches in relation with the structure, *J. Agric. Food Chem.* 48 (2000) 1810–1816.
- [10] C. Orr, Determination of particle size, in: P. Becher (Ed.), *Encyclopedia of Emulsion Technology*, Vol. 3, Marcel Dekker, New York, 1988, chapter 3.
- [11] J. Sjöblom (Ed.), *Encyclopedic Handbook of Emulsion Technology*, Marcel Dekker, New York, 2001.
- [12] B. Balinov, O. Söderman, Emulsions-the NMR perspective, in: J. Sjöblom (Ed.), *Encyclopedic Handbook of Emulsion Technology*, Marcel Dekker, New York, 2001, Chap. 12.
- [13] P. Callaghan, *Principles of Nuclear Magnetic Resonance Microscopy*, Oxford University Press, New York, 1991.
- [14] H.Y. Carr, E.M. Purcell, Effects of diffusion on free precession in nuclear magnetic resonance experiments, *Phys. Rev.* 94 (1954) 630–638.
- [15] S. Meiboom, D. Gill, Modified spin-echo method for measuring nuclear relaxation times, *Rev. Sci. Instrum.* 29 (1959) 688–691.
- [16] E.O. Stejskal, J.E. Tanner, Spin diffusion measurements: spin echoes in the presence of a time-dependent field gradient, *J. Chem. Phys.* 42 (1965) 288–292.
- [17] A.N. Tikhonov, V.Y. Arsenin, *Solution of Ill-Posed Problems*, Winston and Sons, Washington, DC, 1977.
- [18] K.J. Dunn, G.A. LaTorraca, J.L. Warner, D.J. Bergman, On the calculation and interpretation of NMR relaxation times distribution, 69th Annual SPE Technical Conference and Exhibition, New Orleans, USA, 25–28 September (1994), Paper SPE 28367.
- [19] K.R. Brownstein, C.E. Tarr, Importance of classical diffusion in NMR studies of water in biological cells, *Phys. Rev. A* 19 (1979) 2446–2453.
- [20] B. Clark, R.L. Kleinberg, Physics in oil exploration, *Phys. Today* (April 2002) 48–53.
- [21] S. Davies, K.J. Packer, D.R. Roberts, F.O. Zelaya, Pore-size distributions from NMR spin-lattice relaxation data, *Magn. Reson. Imaging* 9 (1991) 681–685.
- [22] C.E. Morriss, J. MacInns, R. Freedman, J. Smaardyk, C. Straley, W.E. Kenyon, H.J. Vinegar, P.N. Tutunjian, Field test of an experimental pulsed nuclear magnetism tool, Transactions of the SPWLA 34th Annual Logging Symposium (1993), Paper GGG.
- [23] R.L. Kleinberg, Utility of NMR T_2 distributions, connection with capillary pressure, clay effect and determination of the surface relaxivity parameter ρ_2 , *Magn. Reson. Imaging* 14 (1996) 761–767.
- [24] W.E. Kenyon, Nuclear magnetic resonance as a petrophysical measurement, *Nuc. Geophys.* 6 (1992) 153–171.
- [25] I. Foley, S.A. Farooqui, R.L. Kleinberg, Effect of paramagnetic ions on NMR relaxation of fluids at solid surfaces, *J. Magn. Reson., Ser. A* 123 (1996) 95–104.
- [26] A. Matteson, J.P. Tomanic, M.M. Herron, D.F. Allen, W.E. Kenyon, NMR relaxation of clay/brine mixtures, *SPE Res. Eval. Eng.* 3 (2000) 408–413.

- [27] R. Freedman, S.W. Lo, M. Flaum, G.J. Hirasaki, A. Matteson, A. Sezginer, A new NMR method of fluid characterization in reservoir rocks: experimental confirmation and simulation results, *SPE J.* (2001) 452–464.
- [28] R. Mills, Self-diffusion in normal and heavy water in the range 1–45°, *J. Phys. Chem.* 77 (1973) 685–688.
- [29] G.A. LaTorraca, K.J. Dunn, P.R. Webber, R.M. Carlson, Low-field NMR determinations of the properties of heavy oils and water-in-oil emulsions, *Magn. Reson. Imaging* 16 (1998) 659–662.
- [30] D.E. Cannon, C. Cao Minh, R.L. Kleinberg, Quantitative NMR interpretation, *SPE Annual Technical Conference and Exhibition*, New Orleans, USA, 27–30 September (1998), SPE Paper 49010.
- [31] Q. Zhang, S.W. Lo, C.C. Huang, G.J. Hirasaki, Some exceptions to the default NMR rock and fluid properties, *SPWLA 39th Annual Logging Symposium*, Keystone, Colorado, May 26–29 (1998), Paper FF.
- [32] R.L. Kleinberg, H.J. Vinegar, NMR properties of reservoir fluids, *Log Analyst* 37 (1996) 20–32.
- [33] K. Allsopp, I. Wright, D. Lastockin, K. Mirotchnik, A. Kantzas, Determination of oil and water compositions of oil/water emulsions using low field NMR relaxometry, *J. Can. Pet. Technol.* 40 (2001) 58–61.
- [34] K.J. Dunn, B. Sun, Personal communication, 2002.
- [35] B.P. Hills, H.R. Tang, P. Manoj, C. Destruel, NMR diffusometry of oil-in-water emulsions, *Magn. Reson. Imaging* 19 (2001) 449–451.
- [36] W.D. Logan, J.P. Horkowitz, R. Laronga, D.W. Cromwell, Practical application of NMR logging in carbonate reservoirs, 1, (1998), 438–448.
- [37] B. Robertson, Spin-echo decay of spins diffusing in a bounded region, *Phys. Rev.* 151 (1966) 273–277.
- [38] C.H. Neuman, Spin echo of spins diffusing in a bounded medium, *J. Chem. Phys.* 60 (1974) 4508–4511.
- [39] J.S. Murday, R.M. Cotts, Self-diffusion coefficient of liquid lithium, *J. Chem. Phys.* 48 (1968) 4938–4945.
- [40] B. Balinov, B. Jönsson, P. Linse, O. Söderman, The NMR self-diffusion method applied to restricted diffusion-simulation of echo attenuation from molecules in spheres and between planes, *J. Magn. Reson. Ser. A* 104 (1993) 17–25.
- [41] K.J. Packer, C. Rees, Pulsed NMR studies of restricted diffusion. I. droplet size distribution in emulsions, *J. Colloid Interface Sci.* 40 (1972) 206–218.
- [42] B. Epstein, Logarithmico-normal distribution in breakage of solids, *Ind. Eng. Chem.* 40 (1948) 2289–2290.
- [43] J.L. Salager, M. Pérez-Sánchez, M. Ramírez-Gouveia, J.M. Andérez, M.I. Briceño-Rivas, Stirring-formulation coupling in emulsions, *Récent Progrés en Génie des Procédés* 11 (1997) 123–130.
- [44] B. Balinov, O. Söderman, T. Warnheim, Determination of water droplet size in margarines and low-calorie spreads by nuclear-magnetic-resonance self-diffusion, *J. Am. Oil Chem. Soc.* 71 (1994) 513–518.
- [45] B. Balinov, O. Urdahl, O. Söderman, J. Sjöblom, Characterization of water-in-crude-oil emulsions by the NMR self-diffusion technique, *Colloid Surf. A-Physicochem. Eng. Asp.* 82 (1994) 173–181.
- [46] J.C. Van Den Enden, D. Waddington, H. Vanaalst, C.G. Vankralingen, K.J. Packer, Rapid determination of water droplet size distributions by PFG-NMR, *J. Colloid Interface Sci.* 140 (1990) 105–113.
- [47] O. Söderman, I. Lönnqvist, B. Balinov, NMR self-diffusion studies of emulsion systems. Droplet sizes and microstructure of the continuous phase, in: J. Sjöblom (Ed.), *Emulsions—A Fundamental and Practical Approach*, Kluwer Academic Publishers, The Netherlands, 1992, pp. 239–258.
- [48] I. Fourel, J.P. Guillemlent, D. Le Botlan, Determination of water droplet size distributions by low-resolution PFG-NMR 1. ‘Liquid’ emulsions, *J. Colloid Interface Sci.* 164 (1994) 48–53.
- [49] I. Fourel, J.P. Guillemlent, D. Le Botlan, Determination of water droplet size distributions by low-resolution PFG-NMR. 2. Solid emulsions, *J. Colloid Interface Sci.* 169 (1995) 119–124.

- [50] H.Y. Lee, M.J. McCarthy, S.R. Dungan, Experimental characterization of emulsion formation and coalescence by nuclear magnetic resonance restricted diffusion techniques, *J. Am. Oil Chem. Soc.* 75 (1998) 463–475.
- [51] M.L. Johns, L.F. Gladden, Sizing of emulsion droplets under flow using flow-compensating NMR-PFG techniques, *J. Magn. Reson.* 154 (2002) 142–145.
- [52] I. Lönnqvist, B. Håkansson, B. Balinov, O. Söderman, NMR self-diffusion studies of the water and the oil components in a W/O/W emulsion, *J. Colloid Interface Sci.* 192 (1997) 66–73.
- [53] C. Orr, Emulsion droplet size data, in: P. Becher (Ed.), *Encyclopedia of Emulsion Technology*, Vol. 1, Marcel Dekker, New York, 1983, pp. 369–404.
- [54] L. Ambrosone, A. Ceglie, G. Colafemmina, G. Palazzo, NMR studies of food emulsions: the dispersed phase self-diffusion coefficient calculated by the least variance method, *Prog. Colloid Polym. Sci.* 115 (2000) 161–165.
- [55] L. Ambrosone, G. Colafemmina, M. Giustini, G. Palazzo, A. Ceglie, Size distribution in emulsions, *Prog. Colloid Polym. Sci.* 112 (1999) 86–88.
- [56] J.E. Tanner, E.O. Stejskal, Restricted self-diffusion of protons in colloidal systems by the pulsed-gradient, spin-echo method, *J. Chem. Phys.* 49 (1968) 1768–1777.
- [57] D.J. Bergman, K.J. Dunn, Theory of diffusion in a porous-medium with applications to pulsed-field-gradient NMR, *Phys. Rev. B* 50 (1994) 9153–9156.
- [58] M.D. Hürlimann, K.G. Helmer, L.L. Latour, C.H. Sotak, Restricted diffusion in sedimentary-rocks-determination of surface-area-to-volume ratio and surface relaxivity, *J. Magn. Reson. Ser. A* 111 (1994) 169–178.
- [59] L.L. Latour, K. Svoboda, P.P. Mitra, C.H. Sotak, Time-dependent diffusion of water in a biological model system, *Proc. Natl. Acad. Sci. USA* 91 (1994) 1229–1233.
- [60] D. Topgaard, O. Söderman, Diffusion of water absorbed in cellulose fibers studied with ¹H-NMR, *Langmuir* 17 (2001) 2694–2702.
- [61] W. Ngwa, O. Geier, L. Naji, J. Schiller, K. Arnold, Cation diffusion in cartilage measured by pulsed field gradient NMR, *Eur. Biophys. J.* 31 (2002) 73–80.
- [62] B. Håkansson, R. Pons, O. Söderman, Structure determination of a highly concentrated W/O emulsion using pulsed-field-gradient spin-echo nuclear magnetic resonance ‘diffusion diffractograms’, *Langmuir* 15 (1999) 988–991.
- [63] B. Balinov, O. Söderman, J.C. Ravey, Diffraction-like effects observed in the PGSE experiment when applied to a highly concentrated water/oil emulsion, *J. Phys. Chem.* 98 (1994) 393–395.
- [64] O. Söderman, U. Olsson, Dynamics of amphiphilic systems studied using NMR relaxation and pulsed field gradient experiments, *Curr. Opin. Colloid Interface Sci.* 2 (1997) 131–136.
- [65] M. Giustini, G. Palazzo, A. Ceglie, J. Eastoe, A. Bumujdad, R.K. Heenan, Studies of cationic anionic surfactant mixed microemulsions by small-angle neutron scattering and pulsed field gradient NMR, *Prog. Colloid Polym. Sci.* 115 (2000) 25–30.
- [66] O. Söderman, M. Nydén, NMR in microemulsions. NMR translational diffusion studies of a model microemulsion, *Colloid Surf. A-Physicochem. Eng. Asp.* 158 (1999) 273–280.
- [67] H. Wennerström, O. Söderman, U. Olsson, B. Lindman, Macroemulsions vs. microemulsions, *Colloid Surf. A-Physicochem. Eng. Asp.* 123 (1997) 13–26.
- [68] J.E. Tanner, Use of the stimulated echo in NMR diffusion studies, *J. Chem. Phys.* 52 (1970) 2523–2526.
- [69] S.J. Gibbs, C.S. Johnson Jr, A PFG NMR experiment for accurate diffusion and flow studies in the presence of eddy currents, *J. Magn. Reson.* 93 (1991) 395–402.
- [70] P. Stilbs, Fourier transform pulsed-gradient spin-echo studies of molecular diffusion, *Prog. NMR Spectrosc.* 19 (1987) 1–45.
- [71] O. Söderman, P. Stilbs, NMR studies of complex surfactant systems, *Prog. NMR Spectrosc.* 26 (1994) 445–482.
- [72] I. Lönnqvist, A. Khan, O. Söderman, Characterization of emulsions by NMR methods, *J. Colloid Interface Sci.* 144 (1991) 401–411.
- [73] B. Jönsson, H. Wennerström, P.G. Nilsson, P. Linse, Self-diffusion of small molecules in colloidal systems, *Colloid Polym. Sci.* 264 (1986) 77–88.

- [74] M.H. Bles, J.C. Leyte, The effective translational self-diffusion coefficient of small molecules in colloidal crystals of spherical particles, *J. Colloid Interface Sci.* 116 (1994) 118–127.
- [75] H. Jóhannesson, B. Halle, Solvent diffusion in ordered macrofluids: a stochastic simulation study of the obstruction effect, *J. Chem. Phys.* 104 (1996) 6807–6817.
- [76] H. Peterlik, D. Loidl, Bimodal strength distributions and flaw populations of ceramics and fibres, *Eng. Fract. Mec.* 68 (2001) 253–261.
- [77] C.C. Huang, Estimation of rock properties by NMR relaxation methods, M.Sc. Thesis, Rice University, Houston, USA, 1997.
- [78] W.H. Press, S.A. Teukolsky, W.T. Vetterling, B.P. Flannery, *Numerical Recipes in FORTRAN: The Art of Scientific Computing*, Cambridge University Press, Cambridge, UK, 1992.
- [79] M. Abramowitz, J. Stegun (Eds.), *Handbook of Mathematical Functions, with Formulas, Graphs and Mathematical Tables*, Dover Publications, New York, 1965.
- [80] L. Wen, K.D. Papadopoulos, Visualization of water transport in $W_1/O/W_2$ emulsions, *Colloids Surf. A-Phys. Chem. Eng. Aspects* 174 (2000) 159–167.
- [81] W. Dixon, F. Massey, *Introduction to Statistical Analysis*, McGraw-Hill, New York, 1957.
- [82] Y. Zhang, G.J. Hirasaki, W. House, R. Kobayashi, Oil and gas NMR properties: the light and heavy ends, SPWLA 43rd Annual Logging Symposium, Oiso, Japan (2002), Paper HHH.
- [83] S. Godefroy, J.P. Korb, M. Fleury, R.G. Bryant, Surface nuclear magnetic relaxation and dynamics of water and oil in macroporous media, *Phys. Rev. E* (2001) 6402, Art. # 021605.
- [84] P. Callaghan, A simple matrix formalism for spin echo analysis of restricted diffusion under generalized gradient waveforms, *J. Magn. Reson.* 129 (1997) 74–84.
- [85] S.L. Codd, P.T. Callaghan, Spin echo analysis of restricted diffusion under generalized gradient waveforms: Planar, cylindrical and spherical pores with wall relaxivity, *J. Magn. Reson.* 137 (1999) 358–372.